International Journal of Hydrogen Energy 138 (2025) 491–508

Contents lists available at ScienceDirect

International Journal of Hydrogen Energy

journal homepage: www.elsevier.com/locate/he

Modeling the impact of temperature-dependent thermal conductivity on hydrogen desorption from magnesium hydride

Davoud Abdi Lanbaran [a,*], Chao Wang [a], Chuang Wen [b], Zhen Wu [c], Bo Li [d]

[a] School of Engineering, University of Kent, UK
[b] School of Construction Management and Engineering, University of Reading, UK
[c] Department of Process Equipment and Control Engineering, Xi'an Jiaotong University, China
[d] School of Electrical, Electronic and Mechanical Engineering, University of Bristol, UK

ARTICLE INFO

Keywords:
Thermal conductivity
Temperature dependence
Hydrogen desorption
Magnesium hydride
Heat transfer efficiency

ABSTRACT

Hydrogen desorption from metal hydrides, especially magnesium hydrides, presents a major challenge in hydrogen storage applications due to their low thermal conductivity and high hydrogen release temperature. Efficient hydrogen release is crucial for operation, as thermal conductivity is key in heat transfer and desorption kinetics. Previous studies have largely assumed a constant thermal conductivity, but considering its temperature dependence is essential for accurate modeling and optimization of the process. In this study, a numerical evaluation of temperature-dependent thermal conductivity in hydrogen desorption from magnesium hydride was conducted using COMSOL Multiphysics and the finite element method (FEM). Two distinct methods, thermochemical storage systems (TCSS) and radial heat flux were investigated under slow and fast hydrogen release conditions. The results show that accounting for temperature-dependent thermal conductivity significantly reduces desorption time, shortening it by approximately 9 min in slow desorption processes and 0.6 min in fast desorption compared to constant thermal conductivity models. Furthermore, the temperature-dependent model enhanced heat distribution, leading to a lower equilibrium pressure of 1.96 MPa (MPa) compared to 2.09 MPa in constant models, and accelerated hydrogen release, as demonstrated by an increase in Darcy's velocity. The findings suggest that incorporating temperature-dependent thermal conductivity in hydrogen storage models is essential for improving heat transfer efficiency, optimizing desorption kinetics, and enhancing overall system performance. These insights will aid in the development of hydrogen storage in metal hydrides and contribute to more accurate predictions of hydrogen storage system performance.

1. Introduction

Renewable energy sources have become increasingly important in modern energy systems due to their role in providing clean, sustainable, and stable power solutions and managing the challenges of the 21st century energy crisis and environmental pollution. Among these, hydrogen is widely recognized as a high-capacity energy carrier with significant potential for large-scale energy storage and conversion [1]. Solid-state hydrogen storage has drawn substantial research attention due to its safety and high volumetric density compared to gas and liquid storage [2,3]. Various materials have been explored for solid-state hydrogen storage, including lithium, sodium, and titanium-based hydrides such as LiH (Lithium hydride), $NaBH_4$ (Sodium borohydride), and TiH_2 (Titanium hydride), each offering distinct advantages such as high hydrogen capacity and low release temperatures [4]. However, magnesium hydride (MgH_2) has gained particular interest due to its high hydrogen storage capacity (~7.6 wt%) relative to its weight, cost-effectiveness, and chemical stability [5,6]. Despite these advantages, MgH_2 presents key challenges, primarily its high hydrogen desorption temperature and high activation energy, which hinder practical applications [7]. Moreover, its low thermal conductivity significantly impacts heat transfer efficiency, resulting in non-uniform heat distribution during hydrogen desorption, which in turn limits the release rate and overall system efficiency [8,9]. As the hydride heats up and begins to desorb hydrogen, its rising thermal conductivity creates a positive feedback: heat spreads more effectively, accelerating further desorption. Additionally, the phase transformation from MgH_2 to $Mg + H_2$ at 500–600 K alters microstructure and thermal transport properties,

* Corresponding author
E-mail address: da562@kent.ac.uk (D. Abdi Lanbaran).

https://doi.org/10.1016/j.ijhydene.2025.05.128
Received 3 March 2025; Received in revised form 28 April 2025; Accepted 8 May 2025
Available online 21 May 2025

affecting heat transfer efficiency in the desorption process [10]. As a result, low thermal conductivity is considered a crucial factor that increases hydrogen release temperatures and decreases activation efficiency [11]. To overcome these limitations, enhancing the thermal conductivity of magnesium hydride has been a central research focus, as increased thermal conductivity can significantly accelerate the desorption process and improve the overall efficiency of MgH_2 in hydrogen storage applications [12]. It is hypothesized that accounting for the increase in MgH_2's thermal conductivity with temperature will result in faster hydrogen desorption rates and more uniform temperature profiles, compared to the traditional constant-conductivity assumption (see Tables 3–6).

Several studies have explored methods to improve the thermal conductivity of magnesium hydride. Popilevsky et al. [13] examined the addition of multi-walled carbon nanotubes (MWCNTs) to magnesium composites, demonstrating a 20 % increase in thermal conductivity compared to pure magnesium. Similarly, Kumar et al. [14] investigated thermochemical energy storage in an Mg + 5 wt% $LaNi_{46}Al_{0.4}$ composite, showing improved heat transfer using plate-making techniques and a 3D copper mesh structure. Yoshida et al. [15] experimentally analyzed hydrogen desorption from MgH_2 using convective heat transfer from a hot gas stream, finding that a 1.4-fold increase in thermal conductivity improved energy efficiency by 12 %, while a doubled argon flow rate raised efficiency by 21 %.

Beyond thermal conductivity enhancement, research has shown that metal hydride tank performance also depends on thermal conductivity directionality, grain size, and porosity [16]. Thongtan et al. [17] demonstrated that in cylindrical MgH_2-based storage tanks, thermal conductivity varies between axial and radial directions, influencing hydrogen release rates. Yoshida et al. [18] further optimized heat transfer by arranging porous MgH_2 sheets in parallel and heating them with hot hydrogen flow, reducing the total desorption time to 103 min. Additionally, reducing grain size and optimizing porous structures have been found to significantly improve heat transfer and hydrogen release kinetics [19].

Although many studies assume a constant thermal conductivity for metal hydrides to simplify numerical simulations, this simplification may not fully capture the material's thermal behavior, particularly in MgH_2, where thermal conductivity is known to vary with temperature and undergo changes during phase transitions [20,21]. Larpruenrudee et al. [22] highlighted that enhancing thermal conditions within magnesium-based hydride systems plays a vital role in accelerating hydrogen absorption and improving overall storage performance. Several experimental and numerical studies have highlighted the importance of incorporating temperature-dependent thermal conductivity in order to improve the accuracy of thermal modeling in hydrogen storage systems [23,24]. Shen and Zhao [25] modeled the transient heat and mass transfer process in MgH_2/Mg systems and found that accounting for this temperature dependence provides better agreement with observed desorption behavior. The hydrogen desorption range of 500–600 K introduces notable physical and chemical changes, which significantly impact heat transfer mechanisms [26]. As described in thermal behavior studies of hydride systems [27,28], these changes include latent heat effects, porosity evolution, and phase transformation, all of which influence effective thermal conductivity. Bennett et al. [29] demonstrated that models with constant thermal conductivity may lead to deviations in predicting transient heat transfer, while temperature-dependent models tend to align more closely with experimental outcomes. Notably, while most studies report that MgH_2 thermal conductivity increases with temperature [13] observed that pure magnesium exhibits a decreasing trend, underlining the need for continued validation through both experimental and numerical approaches [30]. This distinction between metallic and hydride phases is key to understanding their differing thermal transport mechanisms [31].

In this study, we present a systematic investigation of the temperature dependence of thermal conductivity during the hydrogen desorption process in MgH_2. Unlike previous studies that often assume a constant thermal conductivity, this research evaluates its dynamic variation under different thermal conditions, considering both fast and slow desorption processes. The novelty of this study lies in analyzing how temperature-dependent thermal conductivity influences hydrogen release kinetics and overall system performance. Because no single formula exists for MgH_2's thermal conductivity as a function of temperature, we aggregate literature data and use effective medium theory to derive an experimental correlation. This approach allows us to incorporate the impact of structural and phase changes on heat transfer, leading to more accurate modeling and predictions of hydrogen desorption behavior. By deriving temperature-dependent formulas for thermal conductivity, this work provides a more precise and realistic framework for modeling heat transfer in MgH_2 storage systems. These findings contribute to optimizing hydrogen storage technologies and improving their efficiency for practical applications.

2. Methodology

2.1. Geometry and material description

In this study, numerical simulations were conducted to investigate the hydrogen release process from magnesium hydride (MgH_2) structures using COMSOL Multiphysics software, which employs the finite element method (FEM) for computational analysis. The simulations focused on temperature-dependent thermal behavior under different conditions and were designed to assess the influence of thermal conductivity variations on hydrogen desorption. Two distinct geometries, as shown in Fig. 1, were developed, each representing a different hydrogen release mechanism and heat transfer condition.

The first geometry models a thermochemical storage system (TCSS), which focuses on heat management within magnesium hydride during slow hydrogen desorption. This configuration is designed to simulate low-intensity heat transfer, representing conditions where heat conduction and hydrogen release occur gradually. The second geometry represents a system subjected to radial heat flux, simulating a high-rate hydrogen release scenario. This setup is intended to analyze the effect of intense localized heat fluxes on thermal conductivity and the overall hydrogen desorption rate. Both geometries were modeled in a symmetric two-dimensional domain to optimize computational efficiency while accurately capturing the heat transfer dynamics. The domain consists of a porous magnesium hydride layer with hydrogen gas exit paths at the center, ensuring precise simulation of heat and mass transfer interactions. The boundary conditions were defined to reflect realistic operating conditions, including a fixed boundary surface, convective heat transfer regions, and hydrogen gas inlet/outlet boundaries. Additionally, key parameters such as initial temperature, gas velocity, and hydride temperature were systematically varied to examine their influence on thermal behavior during the desorption process. The physical and thermal properties of the materials used in this study, including density, thermal conductivity, and specific heat capacity, are summarized in Table 1.

These values are derived from experimental data and literature sources on hydrogen storage materials (see Table 2). By incorporating temperature-dependent thermal conductivity, the models enable a more accurate representation of the transient thermal behavior in the magnesium hydride system. These geometries provide a framework for analyzing heat transfer rates, hydrogen release efficiency, and overall system performance under varying temperature conditions.

2.2. Modeling and equations

In the Modeling and Governing Equations section, heat transfer and Darcy's velocity field within porous media are analyzed. The heat transfer equation (Eq. (1)), derived from energy conservation, models heat distribution in the hydrogen storage system [32]:

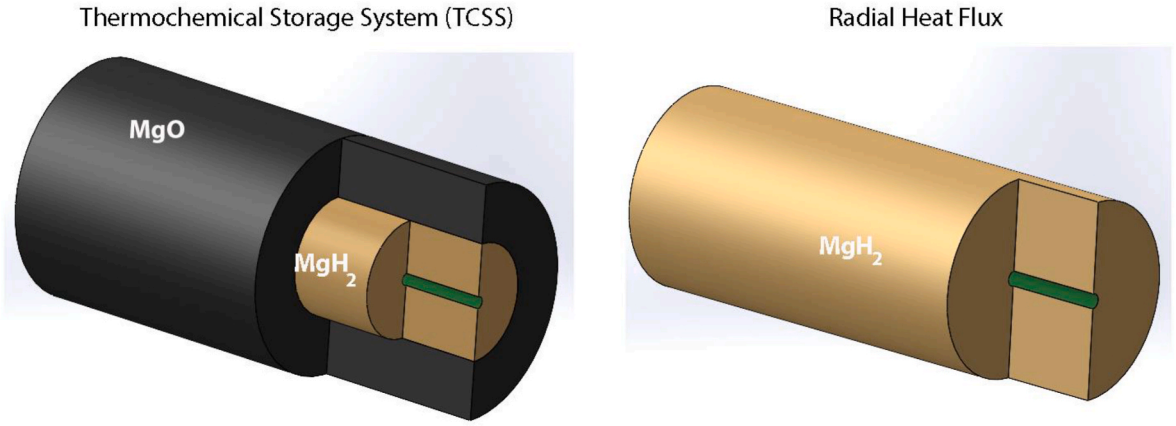

Fig. 1. Schematic geometries for hydrogen desorption under various desorption times.

Table 1
Thermophysical properties of materials.

Description	Value	Symbol	Parameter
Initial pressure	P_0	0.1 MPa	Initial hydrogen pressure in MgH_2
Porosity	ε	0.32	Porosity of MgH_2 bed
Density of magnesium hydride	ρ_{MgH_2}	1450 kg/m^3	Density of MgH_2
Density of magnesium oxide	ρ_{MgO}	3580 kg/m^3	Density of MgO
Density of magnesium hydroxide	$\rho_{Mg(OH)_2}$	2340 kg/m^3	Density of $Mg(OH)_2$
Thermal conductivity of magnesium hydride	λ_{MgH_2}	4.2 W/m·K	Heat transfer capability of MgH_2
Thermal conductivity of magnesium oxide	λ_{MgO}	45 W/m·K	Heat transfer capability of MgO
Thermal conductivity of magnesium hydroxide	$\lambda_{Mg(OH)_2}$	0.55 W/m·K	Heat transfer capability of $Mg(OH)_2$
Specific heat capacity of magnesium hydride	$C_{P\ MgH_2}$	1250 J/kg·K	Heat capacity of MgH_2
Specific heat capacity of magnesium oxide	$C_{P\ MgO}$	880 J/kg·K	Heat capacity of MgO
Specific heat capacity of magnesium hydroxide	$C_{P\ Mg(OH)_2}$	1030 J/kg·K	Heat capacity of $Mg(OH)_2$
Thermal conductivity of hydrogen	λ_{H_2}	0.168 W/m·K	Heat transfer in gaseous hydrogen
Specific heat capacity of hydrogen	$C_{P\ H_2}$	14200 J/kg·K	Heat capacity of hydrogen gas
Thermal conductivity of water	λ_{H_2O}	0.58 W/m·K	Heat transfer in water
Specific heat capacity of water	$C_{P\ H_2O}$	4184 J/kg·K	Heat capacity of water
Activation energy	E_a	41 kJ/mol	Activation energy for hydrogen desorption
Arrhenius pre-exponential factor	A	10 1/s	Arrhenius reaction rate parameter
Hydrogen volume fraction at t = 0	ϕ_{H_2}	1.0	MgH_2 tank is fully saturated with H_2 at t = 0
Water volume fraction at t = 0	ϕ_{H_2O}	0.0	MgO tank is initially empty at t = 0

$$(\rho C_P)_{eff}\frac{\partial T}{\partial t} + (\rho C_P)\mathbf{u}.\nabla T = \nabla\cdot(\lambda\nabla T) + \dot{Q} \quad (1)$$

Here, $(\rho C_P)_{eff}$ is the effective heat capacity (J/m^3·K), $\frac{\partial T}{\partial t}$ is the temperature change over time (K/s), ρC_P is the heat capacity of the fluid (J/m^3·K), u is the fluid velocity (m/s), and ∇T is the temperature gradient (K/m). The term $\nabla\cdot(k\nabla T)$ represents heat conduction (W/ m3), where λ is thermal conductivity (W/m·K), and $\dot{Q}$ is the heat generation rate (W/m3). It is important to distinguish between the effective heat capacity, $(\rho C_P)_{eff}$, and the fluid's heat capacity ρC_P. The effective heat capacity, $(\rho C_P)_{eff}$, is a weighted average of the heat capacities of both the solid and fluid phases (accounting for porosity), while ρC_P refers only to the fluid's heat capacity. This distinction is crucial for accurately modeling energy storage and convective heat transfer. This equation captures conductive and convective heat transfer and thermal effects from chemical reactions. The Arrhenius equation (Eq. (2)) describes the hydrogen desorption rate from magnesium hydride [32]:

$$k = A\cdot\exp\left(\frac{-E_a}{RT}\right) \quad (2)$$

where k is the reaction rate (1/s), A is the Arrhenius coefficient (1/s), E_a is activation energy (J/mol), R is the gas constant (8.314 J/mol·K), and T is temperature (K). This equation highlights that reaction rates increase exponentially with temperature, with E_a determining the required activation energy. The mass conservation of hydrogen in the system is governed by the continuity equation (Eq. (3)) [33]:

$$\frac{\partial\rho}{\partial t} + \nabla\cdot(\rho u) = 0 \quad (3)$$

where u is hydrogen velocity (m/s). This equation ensures that hydrogen inflow, volume changes, and evacuation are balanced, preventing mass loss or spontaneous production. The Van't Hoff equation (Eq. (4)) describes the relationship between equilibrium pressure and temperature in hydrogen storage [34]:

$$P_{eq,H_2} = P_{ref}\times\exp\left(\left(\frac{\Delta H_r}{RT}\right) - \left(\frac{\Delta S_r}{R}\right)\right) \quad (4)$$

where P_{eq,H_2} is equilibrium pressure (Pa), P_{ref} is reference pressure (typically 1 atm), ΔH_r is enthalpy change (J/mol), and ΔS_r is entropy change (J/mol·K). This equation is essential for evaluating hydrogen absorption and desorption performance, as these processes strongly depend on temperature and pressure. Hydrogen flow in porous media is described by Darcy's law (Eq. (5)), which models hydrogen diffusion within the metal hydride reservoir [34]:

$$\mathbf{v} = -\frac{\kappa}{\mu}\nabla P \quad (5)$$

where **v** is flow velocity (m/s), κ is permeability, μ is dynamic viscosity, and P is pressure. Darcy's law provides key insights into hydrogen transport through porous structures, directly influencing desorption efficiency. To determine the effective specific heat capacity of the metal hydride system, Eq. (6) is used. It accounts for the contributions of both gas and solid phases in the porous structure, ensuring accurate thermal modeling during hydrogen desorption and storage [35]:

$$(\rho C_P)_{eff} = \varepsilon\rho_g C_{p,g} + (1-\varepsilon)\rho_s C_{p,s} \quad (6)$$

where ε is bed porosity (dimensionless), ρ_g the gas phase density unit kg/m^3, $C_{p,g}$ the specific heat capacity of the gas unit J/ kg· K, ρ_s is the density of the solid phase unit kg/m^3 and finally $C_{p,s}$ is the specific heat capacity of the solid unit J/kg·K.

2.3. Effective thermal conductivity assessment

Several variables influence the magnesium dehydrogenation process during the desorption phase, primarily due to complex chemical reactions and prolonged reaction times. To achieve optimal dehydrogenation, the system requires a significant increase in temperature, typically about 300 °C above ambient temperature. These temperature variations strongly affect the performance and efficiency of hydrogen storage systems. One of the most important parameters affecting this process is the thermal conductivity of the materials, which varies dynamically with temperature. Given the lack of a comprehensive and unified formula to describe the temperature-dependent thermal conductivity of magnesium-based materials, this study introduces a new modeling approach that combines theoretical formulation and experimental validation. In this model, the system's effective thermal conductivity is expressed as a function of porosity and the temperature-dependent conductivities of the gas and solid phases, as given in Eq. (7) [35].

$$\lambda_{eff} = \varepsilon \times \lambda_{gas}(T) + (1-\varepsilon) \times \lambda_{MH}(T) \tag{7}$$

Here, ε denotes the porosity of the metal hydride structure, $\lambda_{gas}(T)$ is the temperature-dependent thermal conductivity of hydrogen gas, and $\lambda_{MH}(T)$ is the thermal conductivity of the solid hydride material. This formulation enables accurate modeling of heat transfer in a porous hydride bed by incorporating both conduction pathways. The thermal conductivity of hydrogen gas increases with temperature due to enhanced molecular motion and more efficient energy transfer. Experimental expressions for the thermal conductivity of hydrogen and steam were adopted from the studies of Kapischke et al. [35] and Cooper [36].

$$\lambda_{Hydrogen}(T) = 0.171\left(\frac{T}{273.15}\right)^{0.69} \tag{8}$$

$$\lambda_{Steam}(T) = 0.025\left(\frac{T}{298.15}\right)^{0.76} \tag{9}$$

To evaluate the temperature dependence of the solid-phase thermal conductivity, extensive experimental data were collected from the

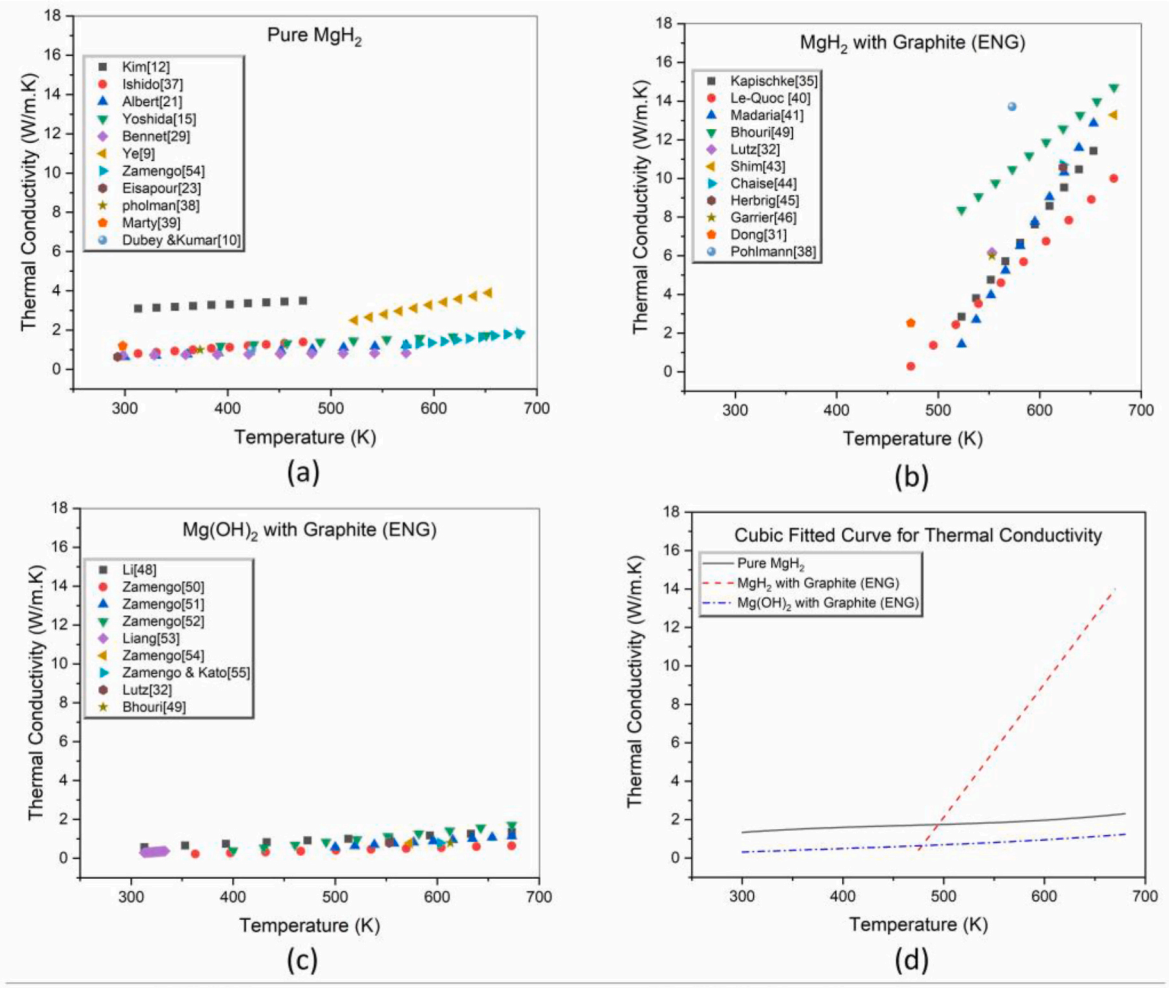

Material	Fitted Cubic Curve Formula
Pure MgH_2	$2.8637 \times 10^{-8}\,T^3 - 3.9685 \times 10^{-5}T^2 + 1.9791 \times 10^{-2}\,T - 1.7988$
MgH_2 with Graphite (ENG)	$-4.8691 \times 10^{-7}\,T^3 + 9.0978 \times 10^{-4}T^2 - 0.5308T + 103.7514$
$Mg(OH)_2$ with Graphite (ENG)	$8.2712 \times 10^{-9}\,T^3 - 9.3661 \times 10^{-6}T^2 + 5.3543 \times 10^{-3}\,T - 0.67357$

Fig. 2. Temperature-dependent thermal conductivity and cubic fitted curve formula.

literature. This dataset covers a wide range of temperatures relevant to the hydrogen desorption process and includes three key materials used for hydrogen storage.

- Pure magnesium [37,38,56].
- Magnesium hydride with expanded natural graphite (ENG) [39–41, 43,45,46].
- Magnesium hydroxide ($Mg(OH)_2$) [47–52,54,55].

Additional reference data from Bhouri and Bürger [42] and Liang [53] were also reviewed, primarily for comparative analysis. The validation dataset, including single-point and multipoint values was adapted from the studies of Lutz et al. [32], Chez et al. [44], Herberg et al. [45], Garrier et al. [46], and Zamengo et al. [50–55]. The collected experimental data were analyzed using a curve-fitting technique. Fig. 2 illustrates the process used to determine the temperature-dependent thermal conductivity profiles. A cubic polynomial fit was applied to the data to accurately reflect the observed nonlinear behavior over a wide temperature range. The resulting experimental formulas, summarized in Fig. 2(d), offer practical expressions for modeling the temperature-dependent thermal conductivity of solid-phase materials in porous hydride systems.

The final integrated models for effective thermal conductivity including the combination of gas and solid phases are presented below for magnesium hydride and magnesium hydroxide:

$$\lambda_{eff(MgH_2)} = \varepsilon \times 0.171\left(\frac{T}{273.15}\right)^{0.69} + (1-\varepsilon)\left(-4.8691\times10^{-7}T^3 + 9.0978\times10^{-4}T^2 - 0.5308T + 103.7514\right) \quad (10)$$

$$\lambda_{eff(Mg(OH_2))} = \varepsilon \times 0.025\left(\frac{T}{298.15}\right)^{0.76} + (1-\varepsilon)\left(8.2712\times10^{-9}T^3 - 9.3661\times10^{-6}T^2 + 5.3543\times10^{-3}T - 0.6735\right) \quad (11)$$

In this formulation, the instantaneous temperature T is the sole variable governing dynamic changes in thermal conductivity during the hydrogen release process. A comprehensive evaluation of the fitting quality-based on R^2 coefficients, absolute error, and relative error is presented in the next section. This validation confirms good agreement between model predictions and experimental results across a wide range of data sources. The resulting model provides a robust and reliable tool for simulating thermal behavior in metal hydride systems and enhancing the accuracy of hydrogen desorption performance predictions. It should be noted that the experimental conductivity correlations obtained here are specific to MgH_2 and its composites (ENG enhanced and $Mg(OH)_2$). Extrapolation to different hydride formulations or new alloys will require additional experimental data and model recalibration. However, the developed method can be applied to other materials in future work.

2.4. Validation of temperature-dependent thermal conductivity model

To verify the accuracy and generalizability of the temperature-dependent thermal conductivity model developed in this study, a comprehensive comparison was conducted using a wide range of experimental datasets reported in the scientific literature. These datasets include single-point and multipoint thermal conductivity measurements for magnesium hydride, its composites, and magnesium hydroxide, covering a broad spectrum of temperatures and structural configurations. The proposed model, presented as Eq. (7) in the main text, was derived through a least-squares polynomial fit applied to experimental thermal conductivity values obtained from eleven independent studies. To evaluate the model's accuracy with respect to the reference data, the following statistical measures were calculated.

- Coefficient of Determination (R^2): To evaluate the accuracy of the fitted model against reference datasets, the coefficient of determination (R^2) was used. This metric quantifies the proportion of variance in the observed data that is explained by the model. It is calculated as:

$$R^2 = 1 - \frac{\sum_{i=1}^{n}(y_i - \acute{y}_i)^2}{\sum_{i=1}^{n}(y_i - \overline{y})^2} \quad (12)$$

Where y_i are the reference (experimental) values, $\acute{y}_i$ are the predicted values from the fitted model, and $\overline{y}$ is the mean of the reference values. An (R^2) value close to 1 indicates a strong agreement between the model and the experimental data and confirms the reliability of the proposed fitting method.

- Absolute error (AE): Absolute difference between predicted and experimental thermal conductivity values:

$$\text{Absolut Error} = \left|\lambda_{\text{Experimental}} - \lambda\right| \quad (13)$$

- Relative error (RE %): Percentage deviation between predicted and experimental values:

$$\text{Relative Error} = \left(\frac{\left|\lambda_{\text{Experimental}} - \lambda\right|}{\lambda_{\text{Experimental}}}\right) \times 100 \quad (14)$$

The results of this analysis are summarized in the Tables 2 and 3 below.

In the meantime, the data reported by Lutz et al. [32], specifically 6.18 W/m·K at 553 K, were selected as a reference for the numerical simulations due to their high level of reliability. The corresponding value predicted by the proposed model at this temperature was 6.33 W/m·K, yielding a small absolute error of 0.15 W/m·K and a relative error of 2.4 %. The datasets from both Lutz et al. [32] and Chaise et al. [44] were also incorporated into Fig. 6 of the main manuscript, as their reported conditions closely matched the boundary conditions applied in our simulation scenarios. These sources provided not only thermal conductivity measurements but also essential operating parameters such as initial temperature and pressure, allowing for consistent numerical validation. Other datasets were excluded from the visual comparison in the main text due to differing experimental assumptions and boundary conditions, which could have introduced discrepancies unrelated to the model's predictive accuracy.

In addition to magnesium hydride and its composites, magnesium hydroxide was also included in the validation process due to its role in system thermal management design strategies. The model showed close alignment with experimental values for $Mg(OH)_2$, confirming its applicability not only to metal hydrides but also to thermochemical energy storage materials. Despite some variances in the literature data especially for advanced composite materials such as ENG-based structures, the model provided consistent and accurate performance fits across most datasets as far as can be seen in Tables 4 and 5. These results confirm that the proposed temperature-dependent thermal conductivity model is suitable for integration into numerical simulations of hydrogen desorption processes and can be used as a predictable and reliable tool in the design and optimization of hydrogen storage.

Table 2
Error and analysis for datasets with multiple experimental points.

Dataset	R^2 Value	Average Absolute Error (W/m·K)	Average Relative Error (%)
Kapischke [35]	0.912	0.54	6.5
Le-Quoc [40]	0.743	1.07	11.2
Madaria [41]	0.862	0.78	8.7
Bhouri [49]	0.431	1.66	16.3

Table 3
Error analysis for datasets with single experimental points.

Dataset	Temperature (K)	Experimental λ	Predicted λ	Absolute Error (W/m.K)	Relative Error (%)
Lutz [32]	553	6.18	6.33	0.15	2.4
Shim [43]	673	13.29	12.51	0.78	5.87
Chaise [44]	623	10.71	10.61	0.10	0.96
Herbrig [45]	623	10.57	10.61	0.04	0.38
Pohlmann [38]	573	13.71	7.94	5.77	42.08
Garrier [46]	553	6.00	6.43	0.43	7.17
Dong [31]	473	2.87	3.04	0.17	5.92

Table 4
Error and analysis for datasets with multiple experimental points.

Dataset	R^2 Value	Average Absolute Error (W/m·K)	Average Relative Error (%)
Zamengo [50]	0.93	0.06	4.57
Zamengo [51]	0.9	0.08	6.21
Zamengo [52]	0.94	0.05	3.77
Liang [53]	0.81	0.17	13.2

2.5. Assumptions

Since this study focuses on the temperature dependence of the thermal conductivity coefficient during hydrogen release, the following assumptions and simplifications were applied in the numerical analysis.

- **Uniform Bed Porosity:**

The porosity of the bed is assumed to be uniform and constant throughout the reaction process. Variations due to particle complexity and non-uniformity are neglected.

- **Local Thermal Equilibrium (LTE):**

The solid and gas phases are assumed to be in local thermal equilibrium at all stages of desorption, simplifying the model by disregarding temperature differences between the two phases.

- **Negligible Radiative Heat Transfer:**

Radiative heat transfer is excluded from the analysis due to its minimal effect on heat conduction in porous substrates.

- **Neglect of Pressure Gradient Effects:**

The impact of pressure gradients on hydrogen desorption is considered negligible and is therefore omitted from the simulation.

- **Adiabatic Reactor Conditions:**

The reactor is assumed to be adiabatic, with no heat exchange between the system and its surroundings.

2.6. Boundary and initial conditions

This section outlines the boundary conditions governing the hydrogen release process in magnesium hydride for the two geometries studied. Fig. 3 illustrates the boundary conditions for each case, while Table 6 provides a summary of the corresponding values and relationships for each boundary.

These conditions are integral to modeling the hydrogen release process in magnesium hydride systems and form the foundation for heat and mass transfer analysis across the three cases. Moreover, the numerical simulation was initiated with well-defined baseline conditions to ensure consistency in modeling the hydrogen desorption dynamics. The entire computational domain was set to an initial temperature of 553 K, representing the preheated state before desorption begins. The system's initial pressure was defined as 0.1 MPa, corresponding to the ambient hydrogen pressure within the metal hydride bed. The porous matrix was assumed to be filled with hydrogen, and the magnesium hydride (MgH_2) phase initially comprising 100 % of the solid phase. The system consists of two interconnected tanks: a magnesium hydride tank and a magnesium oxide tank. At the initial time step (t = 0), the magnesium hydride tank is fully saturated with hydrogen, meaning the hydrogen volume fraction is 1.0. In contrast, the magnesium oxide tank is initially devoid of hydrogen, with a water volume fraction of zero (v = 0.0). As the process begins, water is absorbed into the MgO tank, where it reacts with MgO to form magnesium hydroxide ($Mg(OH)_2$), releasing heat in the process. This heat is subsequently transferred to the magnesium hydride tank, supplying the thermal energy required to initiate hydrogen desorption. This setup simulates a thermochemical storage system in which heat is generated internally rather than supplied externally. These initial conditions establish a reference state for analyzing the impact of temperature-dependent thermal conductivity and various operating conditions on the hydrogen desorption process.

2.7. Research workflow

This section describes the numerical methodology employed in this study, outlining the sequential steps required to establish the initial and boundary conditions necessary for obtaining the final solution. As illustrated in Fig. 4, the analysis follows a structured workflow that involves comparing two different scenarios: one in which the thermal conductivity coefficient is assumed to be constant and another where it is considered temperature-dependent.

The process begins with an initial simulation conducted using a constant thermal conductivity coefficient, and the corresponding results are recorded. Following this, a second simulation is performed using a temperature-dependent thermal conductivity coefficient, taking into

Table 5
Error analysis for datasets with single experimental points.

Dataset	Temperature (K)	Experimental λ	Predicted λ	Absolute Error (W/m.K)	Relative Error (%)
Zamengo [54]	573	1.17	1.2	0.03	2.56
Zamengo & kato [55]	603	1.19	1.23	0.04	3.36
Lutz [32]	553	1.15	1.17	0.02	1.73
Bhouri [49]	613	1.17	1.27	0.1	8.55

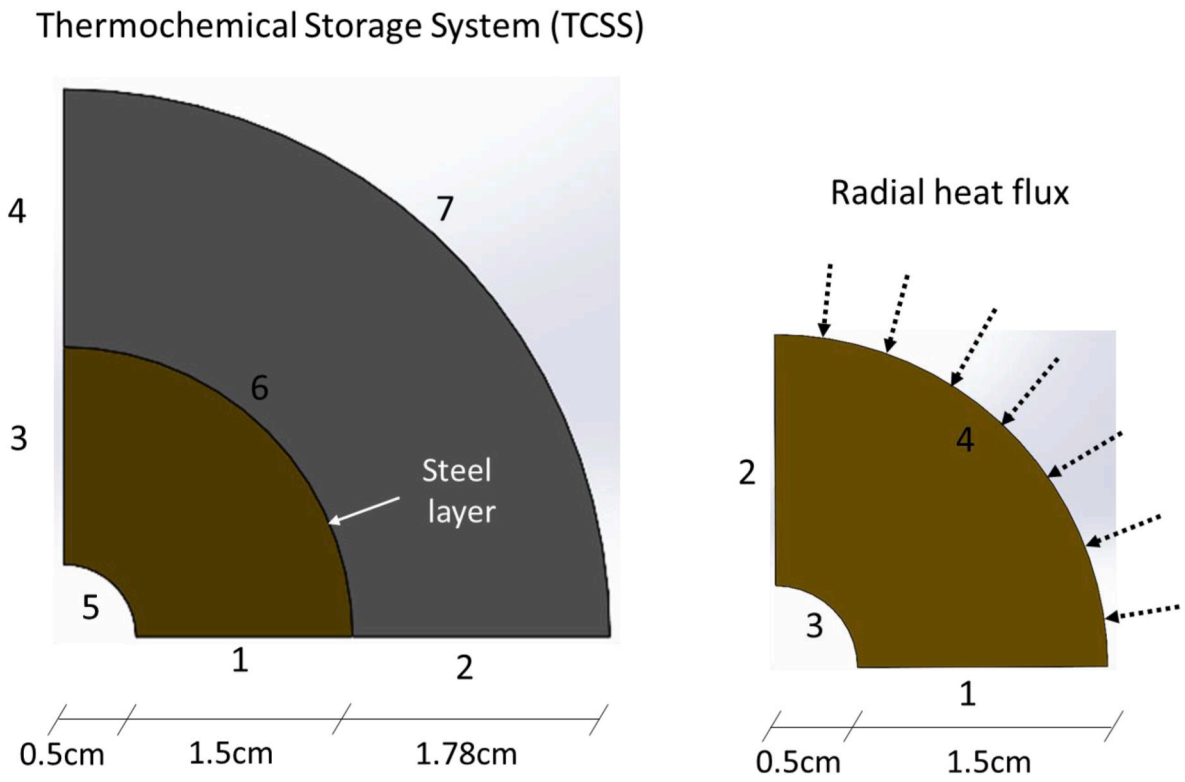

Fig. 3. Geometry and the definition of boundary conditions.

Table 6
Boundary values for each boundary.

Boundary Condition Thermochemical Storage System (TCSS)	Location	Value/Description
Hydrogen outlet pressure	Boundary 5	$P = 1$ bar
Water vapor inlet pressure	Boundary 7	$P = 5$ bar
Thermal insulation	Boundaries 1–5, 7	$\nabla \cdot q = 0$ (no heat flux)
Steel wall heat transfer	Boundary 6	$h = 10{,}000\ W/m^2 \cdot K$
Initial temperature	Entire system	$T_0 = 553$ K
Initial hydrogen pressure	MgH_2 tank	$P_0 = 1.1$ bar
Initial hydrogen Composition	MgO substrate	$x_{h,0} = 0.999, y_{h,0} = 0.001$
Symmetry	Boundaries 1–4	
(Radial heat flux)	**Location**	**Value/Description**
Heat flux	Boundary 4 (case 2)	$q = q_{in} = 6900\ W/m^2$
Thermal insulation	Boundaries 3	$\nabla \cdot q = 0$ (no heat flux)
Symmetry	Boundaries 1–2	

account variations in thermal properties with temperature changes. Once both sets of results are obtained, they are carefully compared against experimental data to evaluate their accuracy. If the temperature-dependent model yields results that closely align with the experimental findings, the methodology is deemed validated, and the process is concluded. However, if discrepancies persist and the simulated results deviate from the experimental observations, the initial conditions and parameters associated with the temperature-dependent thermal conductivity coefficient are redefined, and the simulation is repeated. This iterative approach ensures that the model effectively captures the thermal behavior of the system, with adjustments being made until a high level of agreement with experimental data is achieved, thereby refining the accuracy of the numerical predictions.

2.8. Mesh independence

In this study, two distinct mesh configurations were examined to assess their impact on simulation accuracy and computational efficiency. Both geometries, which were designed for thermochemical material structures and radial heat transfer, respectively, featured symmetrical layouts, making them well-suited for a mapped mesh configuration. The mapped mesh, known for its higher-order accuracy and efficient element distribution, allowed for a reduction in the number of required elements while maintaining precise results. Specifically, accurate and experimentally consistent findings were obtained with just 1824 rectangular elements in the mapped mesh.

To further refine the meshing strategy, five different mesh densities were systematically evaluated. The results indicated that beyond the fourth meshing step, additional refinement did not yield significant improvements in accuracy. In particular, the discrepancies between the fourth and fifth mesh refinements were found to be negligible, confirming that a configuration of 1824 mapped mesh elements was sufficient for reliable simulations. Throughout this evaluation, two critical parameters were continuously monitored: desorption time and the maximum temperature within the metal hydride structure. These variables played a pivotal role in determining the effectiveness of each meshing configuration. As illustrated in Fig. 5, the findings demonstrate that the fourth meshing configuration achieves an optimal balance between computational efficiency and result accuracy, ensuring reliable predictions without unnecessary computational overhead.

3. Result and discussion

3.1. Validation

To ensure the accuracy of the numerical simulations, the results were validated against experimental data by Chaise et al. [44] and numerical studies by Chaise et al. [44] and Lutz et al. [32]. The survey by Chaise et al. [44] provides one of the most comprehensive experimental

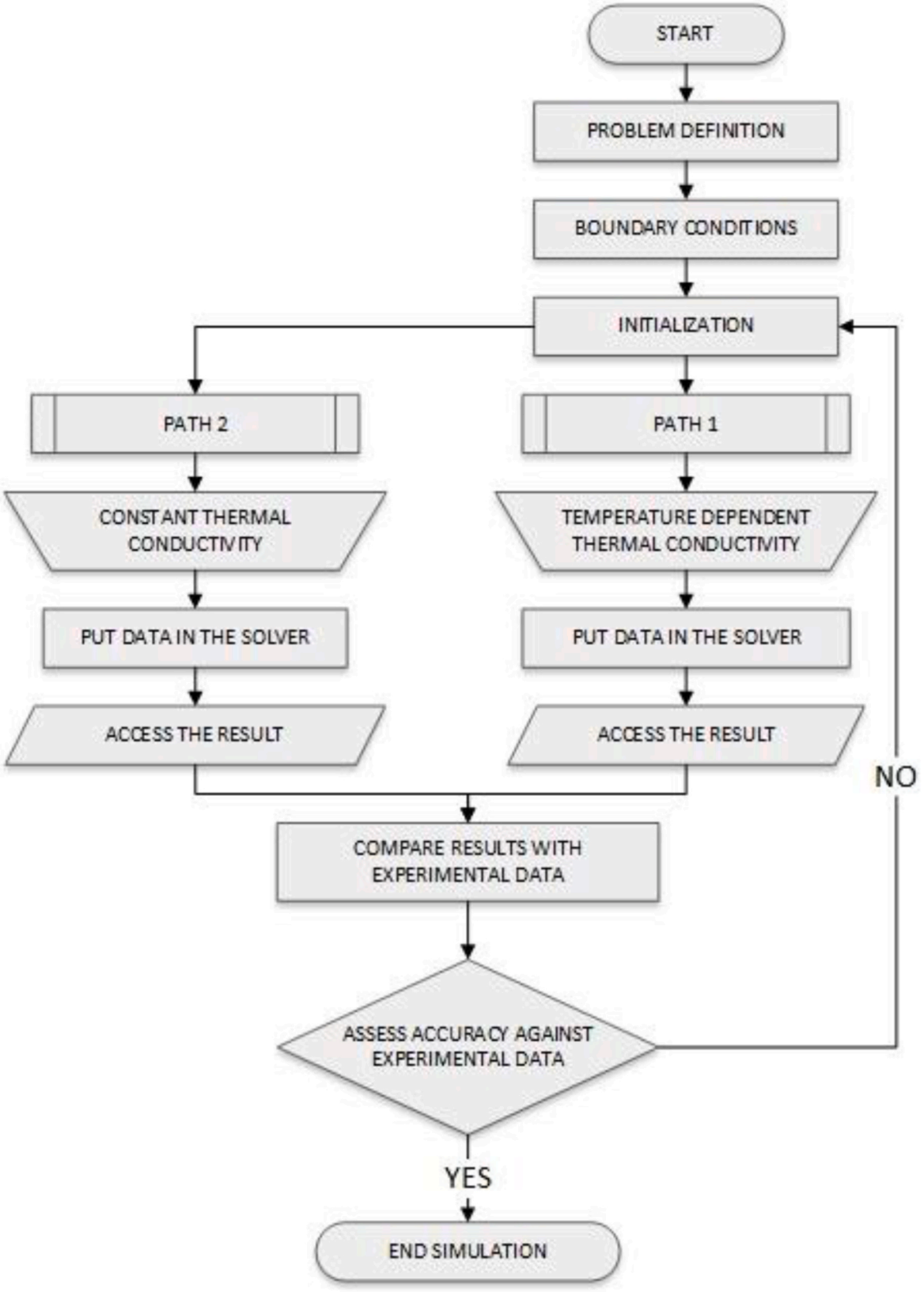

Fig. 4. Methodology of the numerical research.

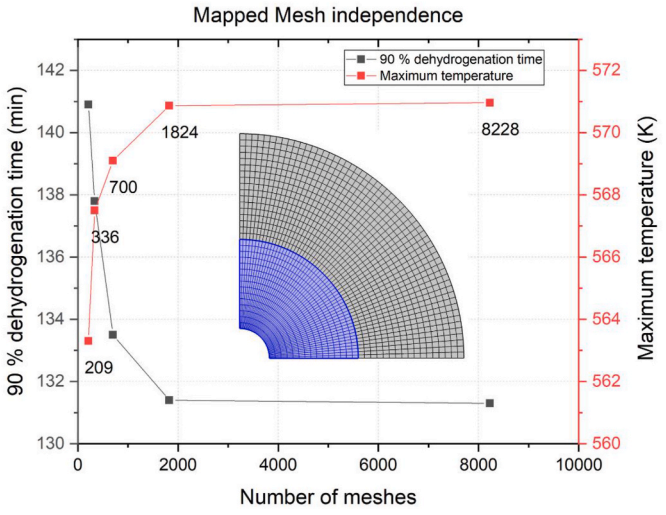

Fig. 5. Mesh independence for both mesh types.

investigations on magnesium hydride reinforced with natural graphite, covering the temperature range of 550–650 K and the pressure range of 1–5 bar, which is fully consistent with the present study. In addition, Lutz et al. [32] performed a numerical analysis focusing on hydrogen release under slow-release conditions, making it a suitable benchmark for comparison. These resources provide a strong basis for validating the temperature, pressure, and hydrogen release volume predicted by the numerical model.

The comparison showed that the numerical model including the temperature-dependent thermal conductivity significantly improves the accuracy of temperature prediction, and the error rate in matching the temperature data is less than 1 %. The simulated temperature trends follow the experimental data with acceptable accuracy and effectively capture the heat transfer in the metal hydride system. Minor deviations occurring over long periods can be attributed to differences in boundary conditions and kinetic interactions in the experimental setup. Apart from temperature, further validation was performed on the volume of desorbed hydrogen, a critical parameter in assessing the effectiveness of the desorption process. The numerical results closely follow the experimental trends, especially in the early stages when heat transfer is dominant in the desorption kinetics. In contrast, the models assuming constant thermal conductivity show larger deviations, emphasizing the importance of temperature-dependent effects in accurately capturing the hydrogen release characteristics. The improved correlation of the temperature-dependent simulations with the experimental data further confirms that the incorporation of dynamic thermal properties is essential for the realistic modeling of hydrogen desorption behavior. Since the temperature-dependent model aligns well with the experimental data, its predictions will be evaluated in two distinct scenarios: slow desorption in a thermochemical storage system and rapid desorption under radial heating.

3.2. *Analysis of thermochemical storage system (TCSS) in slow hydrogen desorption processes*

To optimize energy consumption, thermochemical materials are among the most effective systems for hydrogen storage. However, their inherently low thermal conductivity slows down the hydrogen storage process by delaying the system's adaptation to imposed temperature gradients. During hydrogen desorption, efficient heat distribution is essential to sustain the chemical reactions required for hydrogen release. Increased thermal conductivity enhances heat transfer, promotes a more uniform temperature distribution within the reservoir, accelerates reaction rates, and minimizes localized delays. To investigate this effect, the system was selected as a case study to analyze the impact of temperature-dependent thermal conductivity on the slower desorption processes in MgH_2 and $Mg(OH)_2$. For comparison, the numerical study by Lutz et al. [32] was used as a reference, in which effective constant thermal conductivity values of 4.2 W/m·K for magnesium hydride and 0.55 W/m·K for magnesium hydroxide were assumed, providing a baseline for evaluation.

Fig. 7 presents a comparative analysis of MgH_2 and $Mg(OH)_2$, illustrating their temperature contours (right semicircle) and reaction kinetics (left semicircle). The results indicate that a significant portion of the reaction kinetics is completed within 150 min. Considerably, the magnesium hydride system exhibits faster kinetics, with most of the reaction concluding within 120 min, whereas in magnesium hydroxide, the reaction extends to approximately 150 min. This accelerated reaction in the magnesium hydride system is primarily attributed to its higher thermal conductivity, which facilitates more efficient heat transfer. The magnesium hydroxide environment generates a sharper temperature gradient (40 K) that persists for up to 240 min, whereas in the magnesium hydride system, the temperature gradient is approximately 20 K. These findings demonstrate that higher thermal conductivity contributes to a more uniform temperature distribution, which is essential for optimizing heat transfer and hydrogen desorption during heat exchange and the skin-shell reaction. These comparisons

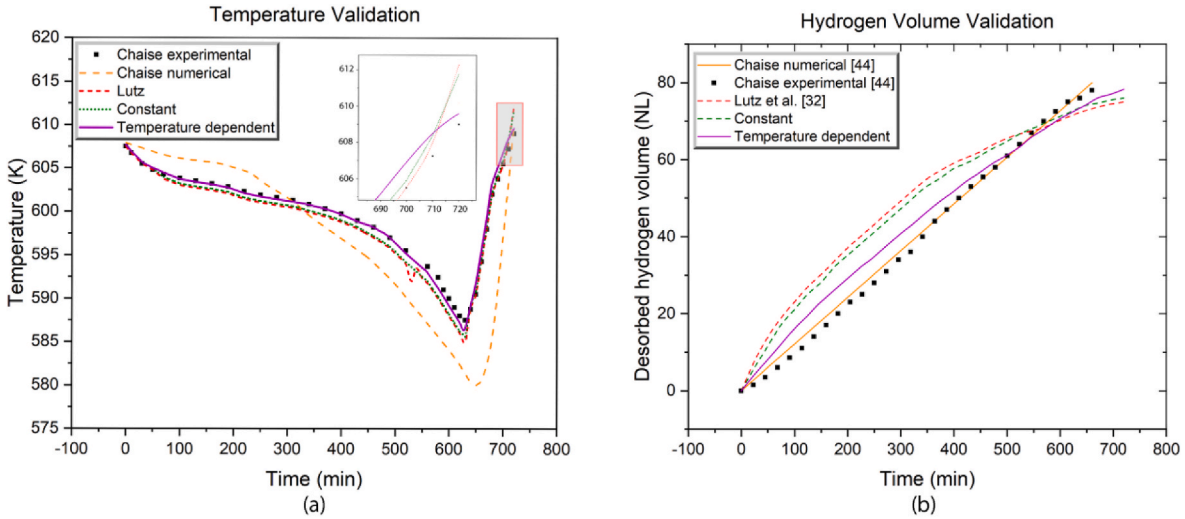

Fig. 6. Numerical analysis validation.

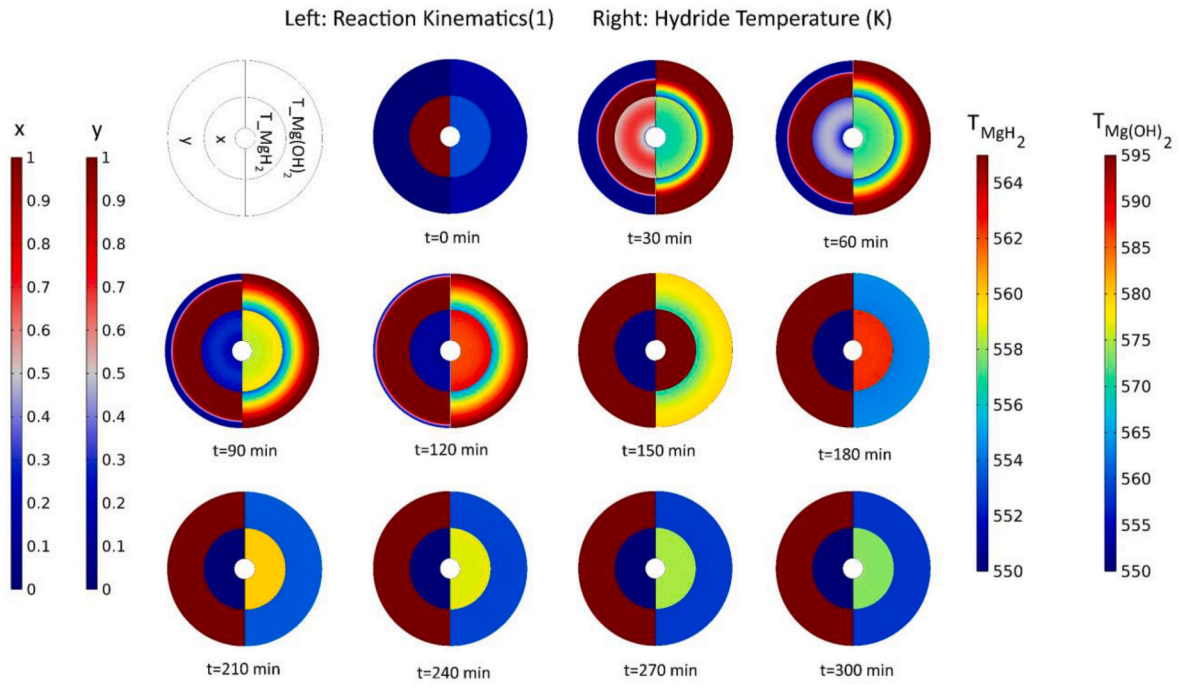

Fig. 7. Temperature and reaction kinetics contours for thermochemical storage system (TCSS).

underscore the critical influence of thermal conductivity on reaction kinetics and highlight the necessity of incorporating temperature-dependent thermal conductivity models to enhance the accuracy of numerical simulations for hydrogen storage materials.

Fig. 8(a) illustrates the process of analyzing two key aspects of magnesium hydride (MgH_2) decomposition: the reaction kinetics and the material's temperature profile during hydrogen release. This analysis evaluates the role of temperature-dependent thermal conductivity in influencing heat transfer and reaction rates. The results indicate that when a variable thermal conductivity coefficient is applied, the conversion rate of MgH_2 to Mg increases significantly, underscoring the importance of incorporating this parameter in kinetic modeling. To compare constant and temperature-dependent thermal conductivity models, simulations introduce the concept of average temperature (T_{ave}) as a reference point. Given the substantial difference between initial and peak temperatures in metal hydride tanks, using only the initial temperature to define a constant conductivity value may lead to oscillations in simulation results and discrepancies from experimental data. To mitigate these issues, T_{ave} is calculated as:

$$T_{ave} = \frac{T_{max} + T_{min}}{2} \tag{15}$$

This temperature is then applied in the effective thermal conductivity equations (Eqs. (10) and (11)) to establish a benchmark for comparison with the temperature-dependent model. Implementing T_{ave} in the constant model helps minimize fluctuations and improve agreement between simulation outcomes and experimental data. The impact of temperature-dependent conductivity extends beyond improving heat transfer; it also accelerates hydrogen desorption. In materials such as MgH_2 and magnesium hydroxide reinforced with natural graphite, thermal conductivity increases with rising temperature (as shown in Fig. 2(d)), creating a synergistic effect. Higher temperatures not only enhance molecular kinetic energy and lower activation barriers for chemical reactions but also promote more uniform heat distribution. This ensures a consistent reaction rate throughout the material, preventing localized temperature extremes that can otherwise hinder efficiency. Performance comparisons indicate that 90 % hydrogen

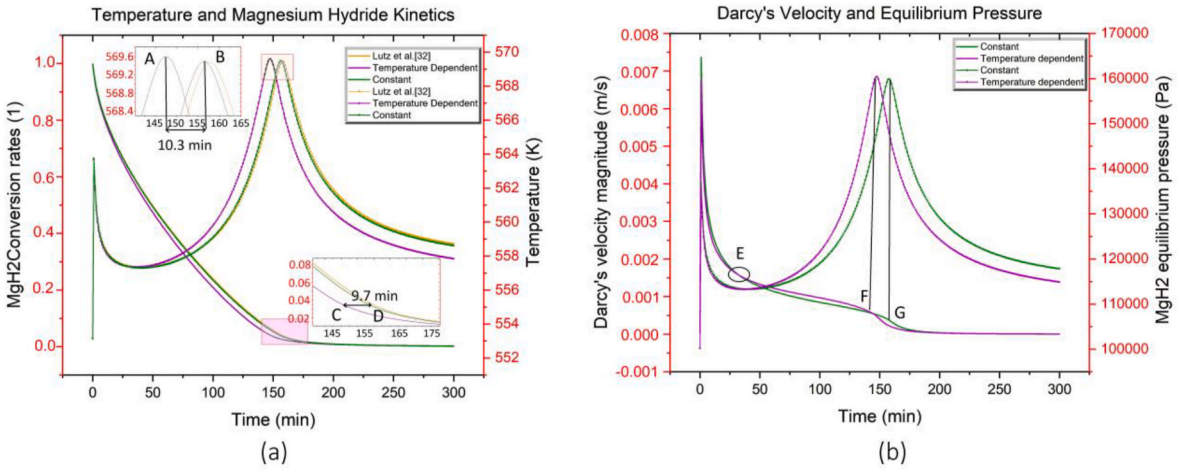

Fig. 8. Temperature and magnesium hydride kinetics diagram.

desorption is achieved in 129 min with temperature-dependent conductivity, whereas it takes 138 min under constant conductivity. Additionally, the temperature-dependent model reduces the time required to reach the maximum temperature, accelerating the overall desorption process. The constant thermal conductivity model limits the heat distribution, which results in a slower desorption process and a longer hydrogen release time. Since the thermal conductivity remains constant, the heat is distributed uniformly but does not adapt to temperature changes, causing some regions to reach the activation temperature required for hydrogen desorption. In contrast, the temperature-dependent thermal conductivity model increases the heat distribution by increasing the conductivity with increasing temperature. This accelerates the heating of the metal hydride and allows more regions to reach desorption conditions sooner. The simulation results, confirmed by experimental data, highlight the advantages of using temperature-dependent models, as they more accurately represent the thermal behavior of the metal hydride system and optimize the hydrogen desorption efficiency.

Fig. 8(b) presents Darcy's velocity and hydrogen pressure variation patterns within the metal hydride tank, comparing the effects of temperature-dependent and constant thermal conductivity in the TCSS system. The pressure pattern mirrors the temperature trends, highlighting the strong correlation between thermal conductivity, heat transfer, and hydrogen desorption dynamics. The results indicate that although both models achieve a maximum pressure of 1.57 MPa, the time required to reach this pressure differs significantly. Under the temperature-dependent model, peak pressure is reached earlier (point F), whereas a noticeable delay occurs with constant conductivity. This earlier pressure build-up results from improved heat distribution: higher temperatures increase conductivity, facilitating more efficient heat spread within the metal hydride. Since Darcy's velocity is directly influenced by the pressure gradient, the more uniform and accelerated heating in the temperature-dependent model enhances the local temperature rise, thereby accelerating hydrogen desorption. Consequently, steeper pressure gradients develop, leading to higher Darcy's velocity. At 25 min (point E), the Darcy velocity under temperature-dependent conductivity reaches 0.0018 m/s, exceeding that of the constant conductivity model. The velocity continues to rise, reaching a maximum of 0.00057 m/s at point F, at which stage hydrogen discharge is nearly complete. In contrast, under constant conductivity, the Darcy velocity increases more gradually, peaking later at point G with a lower value of 0.00044 m/s. This delayed response reflects the limited heat distribution of the constant conductivity model, which slows pressure gradient formation and hydrogen release. The diagrams demonstrate that temperature-dependent thermal conductivity enhances heat distribution, enabling faster pressure build-up and a higher pressure gradient, which in turn increases Darcy's velocity and accelerates hydrogen desorption. Unlike the constant conductivity model, where heat spreads

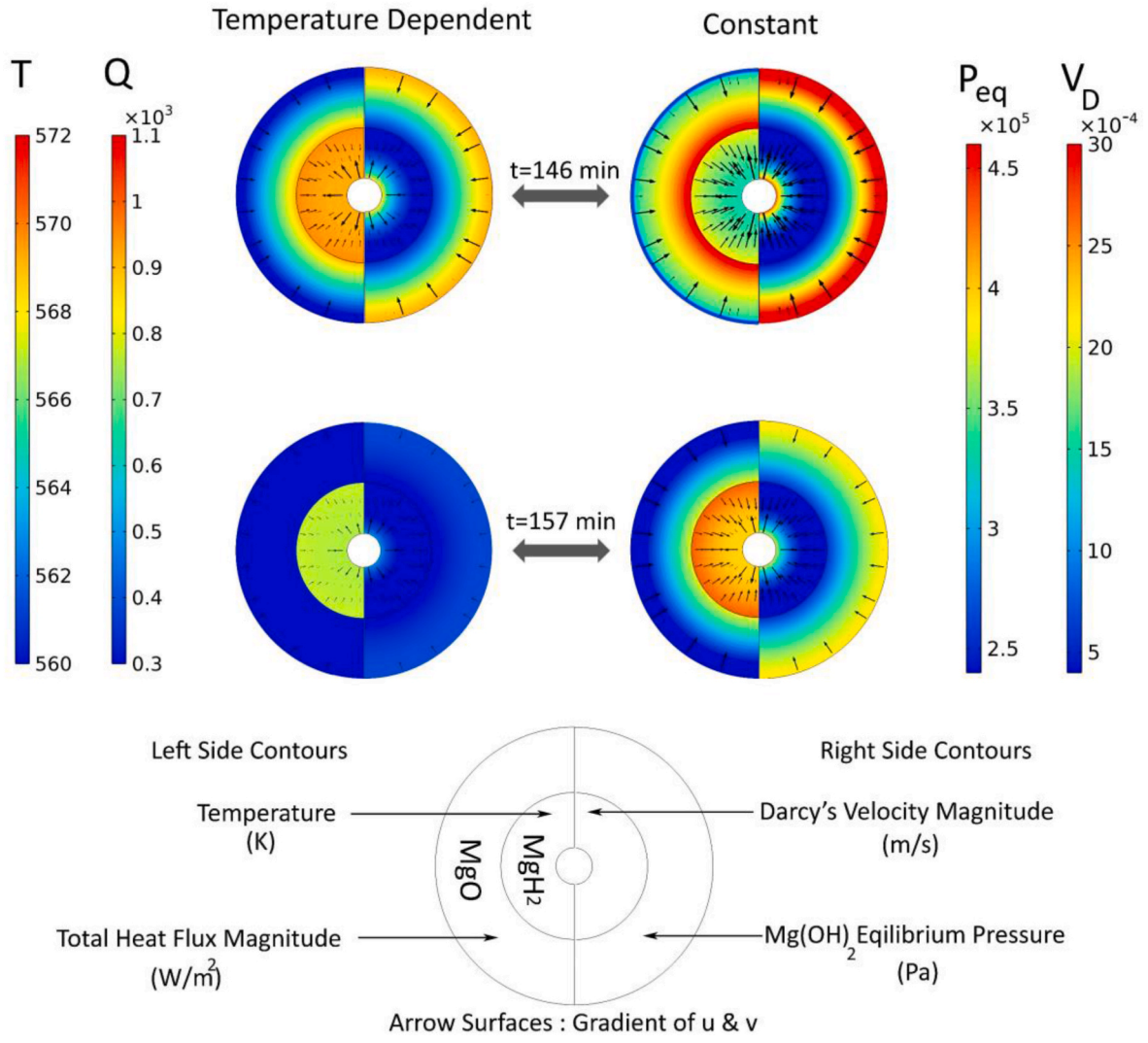

Fig. 9. Temperature and kinetics of thermochemical storage system (TCSS) at two different time steps.

uniformly without adapting to temperature changes, the temperature-dependent model allows heat to diffuse more efficiently as temperature rises, ensuring that more regions reach desorption conditions sooner.

Based on the analysis of the temperature and reaction time curves in Figs. 8(a) and 9, this section examines the graphical contours that illustrate the temperature distribution and reaction kinetics of the magnesium hydride system. Fig. 8(a) highlights key comparison points (A and B) corresponding to different locations within the magnesium hydride structure, while Fig. 9 presents the heat flux paths and pressure variations at the MgH_2–$Mg(OH)_2$ interface. At 143 min, the temperature profile in the magnesium hydride region within the temperature-dependent thermal conductivity model is significantly higher than in the constant conductivity model. This behavior can be explained by the Arrhenius equation (Eq. (2)), which describes the strong temperature dependence of the reaction rate. A more uniform temperature distribution ensures that all regions of the metal hydride are exposed to consistently high temperatures, preventing localized reaction slowdowns and sustaining high material desorption rates. This relationship underscores the crucial role of temperature-dependent thermal conductivity in maintaining optimal reaction conditions and emphasizes the importance of accurately modeling this parameter in hydrogen desorption simulations.

Additionally, the pressure in the magnesium hydroxide region on the right side of the contour view is lower compared to the constant thermal conductivity case. This results in a stronger pressure-driven force at the interface with magnesium hydride, accelerating hydrogen diffusion and increasing the reaction rate. Moreover, the Darcy velocity for magnesium hydride in the temperature-dependent state is considerably higher, indicating a more efficient gas release mechanism under pressure, which further enhances reaction kinetics and accelerates hydrogen desorption. By 157 min, the hydrogen desorption reaction in the temperature-dependent thermal conductivity model is complete, whereas in the constant thermal conductivity model, desorption is still ongoing. This suggests that temperature-dependent thermal conductivity not only accelerates the hydrogen desorption process but also improves overall efficiency compared to the constant model. These findings highlight the crucial role of temperature-dependent thermal conductivity in achieving higher temperatures, enhancing reaction kinetics, and ultimately enabling a more efficient hydrogen decomposition process than when assuming constant thermal conductivity. Accurate temperature-dependent thermal modeling is essential for optimizing hydrogen storage systems, as it improves release efficiency and reduces processing time compared to constant thermal assumptions.

3.3. Radial heat analysis: fast desorption

Unlike the gradual heating in TCSS, the radial heat case imposes a strong heat flux, leading to distinct dynamic behavior, as shown in Figs. 10–12. In this configuration, heat is applied radially, causing a more concentrated and rapid temperature increase, which significantly influences the hydrogen release rate and reaction kinetics. This section analyzes the hydrogen desorption process over a short duration using a radial heat model. A constant heat flux of 6900 W/m^2 was applied radially to evaluate the effectiveness and rate of hydrogen release. Fig. 10 presents the temperature and kinetic contours of magnesium hydride, illustrating temperature variations over time and the corresponding kinetic behavior. The temperature contour highlights variations at different time intervals. During the initial and intermediate stages (0–50 min), the temperature rises uniformly and gradually, reaching 598 K, indicating consistent heat absorption and a steady hydrogen release rate. In the final stage (50–60 min), a sharp temperature increase of approximately 70 K is observed due to significant hydrogen desorption, which leads to heat accumulation and a rapid temperature rise. This behavior underscores the role of thermal conductivity in desorption dynamics.

The kinetic contour of the magnesium hydride reaction in Fig. 10 confirms that hydrogen release is a continuous process. The reaction rate remains steady in the early and middle stages, correlating with uniform temperature increases. However, as hydrogen content decreases toward the end of desorption, the reaction rate slows slightly, aligning with the observed temperature surge. Increasing the heating rate proportionally accelerates desorption, making heat optimization crucial for improving system efficiency while preventing localized overheating.

Fig. 11(a) illustrates how radial heat transfer influences the acceleration of hydrogen desorption in a magnesium hydride tank, particularly under temperature-dependent and constant thermal conductivity conditions. In the early stage of desorption (0–15 min, Block H), both the temperature-dependent and constant thermal conductivity models exhibit similar kinetic behavior due to a relatively small temperature gradient, resulting in comparable heat transfer rates. However, as desorption progresses beyond 50 min, the differences between the two

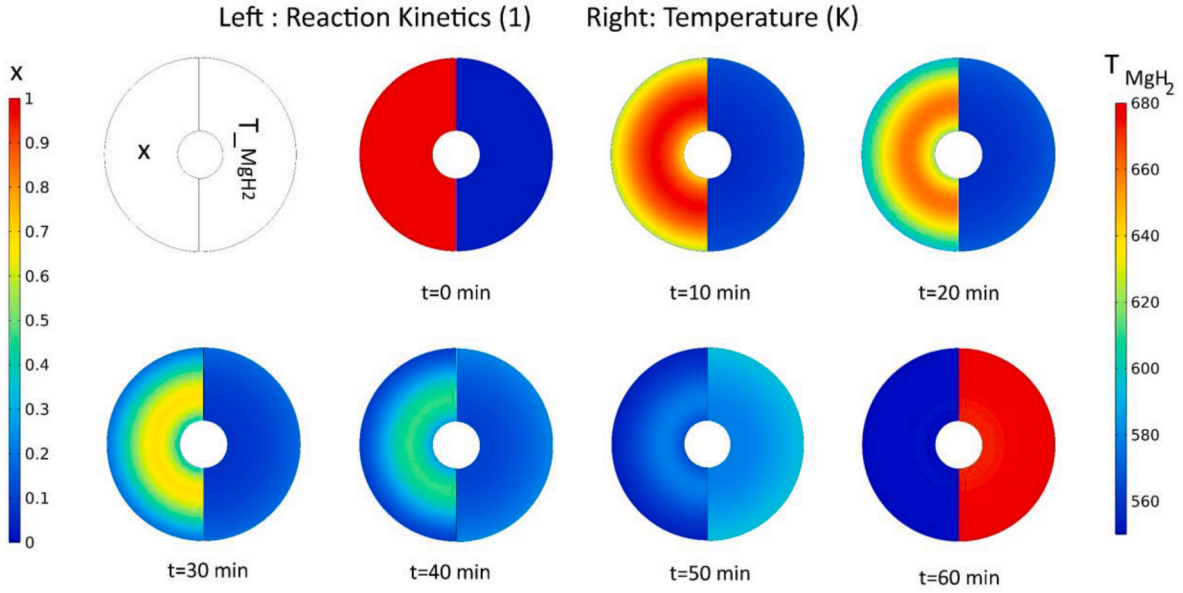

Fig. 10. Temperature and reaction kinetics contours.

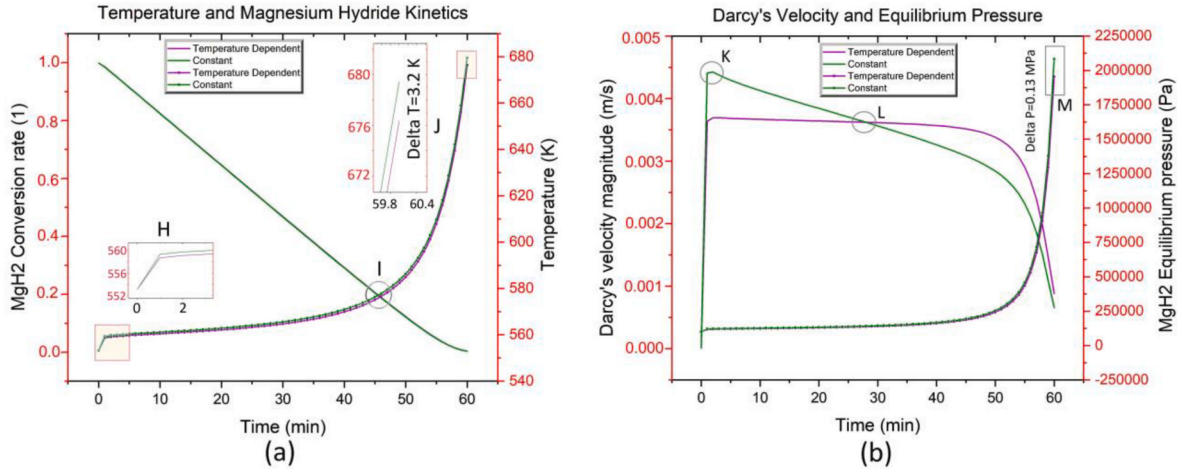

Fig. 11. Temperature vs. Magnesium Hydride Kinetics and Darcy Velocity vs. Equilibrium Pressure for radial heat transfer.

models become more pronounced. The temperature-dependent model enhances heat transfer efficiency and ultimately reduces the desorption time by approximately 0.6 min compared to the constant thermal conductivity model. While this reduction may appear minor, its significance lies not in the duration alone but in the improved heat responsiveness and system behavior it represents. In both models, the same amount of heat is applied, yet the temperature-dependent model adapts more effectively to thermal gradients as desorption advances. This leads to greater desorption responsiveness, smoother pressure propagation, and higher system stability. In large-scale or continuous hydrogen storage systems, such differences accumulate over time and translate into meaningful operational improvements, enhancing cyclic efficiency, reducing thermal stress, and improving real-time system responsiveness under fluctuating input conditions.

In the final phase of desorption (after 90 % hydrogen release, point I), a sharp temperature increase is observed as the depletion of hydrogen alters the heat transfer mechanism, leading to increased thermal resistance and localized heat accumulation. This temperature rise is more pronounced in the temperature-dependent model, reaching approximately 3.2 K higher (Block J) than in the constant thermal conductivity model. This difference arises because, as hydrogen content decreases, thermal resistance increases, causing heat buildup. In contrast, the constant thermal conductivity model, which does not account for temperature variations, exhibits lower heat transfer efficiency, leading to a slightly prolonged desorption process. These findings highlight the critical role of temperature-dependent thermal conductivity in improving heat distribution, preventing localized overheating, and optimizing the thermal performance of hydrogen storage systems.

Fig. 11(b) presents the evolution of Darcy's velocity and equilibrium pressure during hydrogen desorption in magnesium hydride, comparing temperature-dependent and constant thermal conductivity models. Initially, Darcy's velocity in the constant thermal conductivity model increases rapidly, surpassing that of the temperature-dependent model until point K. At this stage, the temperature-dependent model overtakes the constant model due to its enhanced heat transfer capability, which generates a steeper pressure gradient and improves hydrogen mobility. This trend continues until point L, where the temperature-dependent model accelerates hydrogen discharge. However, as hydrogen content declines, the pressure gradient weakens, causing Darcy's velocity in the temperature-dependent case to drop below that of the constant thermal conductivity model. This occurs because of greater heat absorption in the temperature-dependent model, leading to a faster reduction in pressure gradients and a gradual decline in velocity. Throughout most of the desorption process, the equilibrium pressure trends remain similar for both models. However, as shown in the enlarged section at point M, the equilibrium pressure in the constant thermal conductivity model exceeds that of the temperature-dependent model. This difference arises because the constant thermal conductivity model struggles with efficient heat transfer, stabilizing pressure at a higher level. In contrast, the temperature-dependent model facilitates smoother heat dissipation, preventing excessive pressure peaks and ensuring more uniform pressure distribution. The complete hydrogen desorption process occurs in approximately 60 min. After this point, the constant thermal conductivity model results in a higher residual pressure than the temperature-dependent model, with a difference of approximately 0.13 MPa. This disparity is attributed to the heat distribution mechanisms in each case. In the constant thermal conductivity model, heat spreads uniformly, leading to localized pressure buildup. Conversely, the temperature-dependent model optimizes heat dissipation, reducing thermal resistance and ensuring a smoother pressure decline. As a result, in box M, the equilibrium pressure in the constant thermal conductivity model reaches 2.09 MPa, whereas in the temperature-dependent model, it remains at 1.96 MPa. These findings emphasize the crucial role of temperature-dependent thermal conductivity in enhancing system adaptability by dynamically responding to thermal variations. This improved thermal response optimizes pressure and velocity behavior, accelerating hydrogen desorption and ensuring greater efficiency in hydrogen storage systems. Incorporating temperature-dependent models in future designs could significantly improve the performance of hydrogen storage technologies for advanced energy applications.

Fig. 12 presents the evolution of Darcy's velocity and equilibrium pressure in magnesium hydride at three distinct time steps, illustrating how these properties change under temperature-dependent and constant thermal conductivity conditions. At $t = 5$ min, the equilibrium pressure in the constant thermal conductivity model is twice as high as in the temperature-dependent model. This elevated pressure results in a higher Darcy's velocity in the constant model at this stage, as observed in the contour plot. However, as the desorption process advances, the difference in Darcy's velocity between the two models gradually diminishes, leading to a more balanced state by $t = 30$ min. This time interval corresponds to the intersection point in Fig. 7, where Darcy's velocity values for both models become approximately equal.

At the final stage of desorption, when the magnesium hydride tank is fully depleted, the equilibrium pressure remains higher in the constant thermal conductivity model than in the temperature-dependent model. However, Darcy's velocity in the constant model is lower, due to the steeper pressure gradient inside the tank. This results in a non-uniform pressure distribution, which restricts gas velocity and slows hydrogen desorption. The contours at different time steps demonstrate that the evolution of Darcy's velocity and equilibrium pressure under temperature-dependent thermal conductivity follows a smooth and continuous trend, ensuring better thermal distribution and desorption

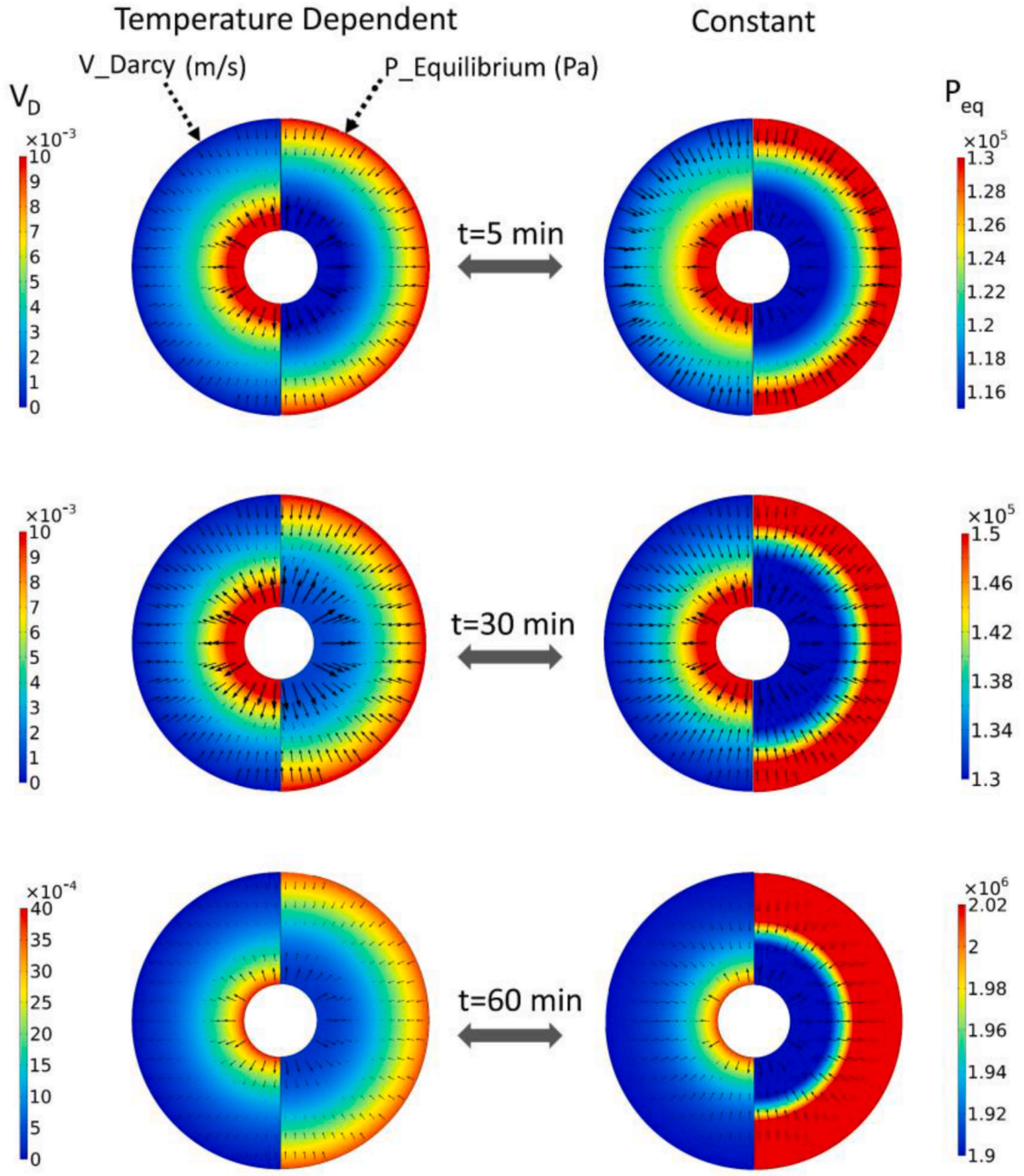

Fig. 12. Darcy's velocity and the equilibrium pressure of radial heat under three distinct time steps.

efficiency. These findings highlight the importance of temperature-dependent thermal conductivity in providing a more accurate and realistic representation of the hydrogen desorption process, aligning closely with experimental observations and real-world storage conditions.

3.4. System behavior under changing initial conditions: a parametric analysis

3.4.1. Parametric analysis for the thermochemical storage system (TCSS)

Fig. 13 presents the effect of initial conditions, specifically variations in temperature and pressure, on the desorption dynamics of a magnesium hydride storage system. The analysis compares how these variations influence desorption time under both constant and temperature-dependent thermal conductivity models. The reference case assumes an initial temperature of 553 K and an initial pressure of 0.1 MPa. To examine temperature effects, incremental changes of ±5 K and ±10 K are introduced. The results indicate that increasing the initial temperature prolongs desorption time, with the effect being more pronounced in the temperature-dependent thermal conductivity model due to its influence on heat transfer dynamics. A 10 K increase extends desorption time by 25 % in the temperature-dependent case and 17 % in the constant thermal conductivity model. Similarly, a 5 K increase results in a moderate extension of desorption time, reinforcing that temperature-dependent thermal conductivity amplifies system sensitivity. Conversely, reducing the initial temperature shortens desorption time, with a stronger impact in the constant thermal conductivity model. A 10 K decrease leads to an 18 % reduction in desorption time under constant

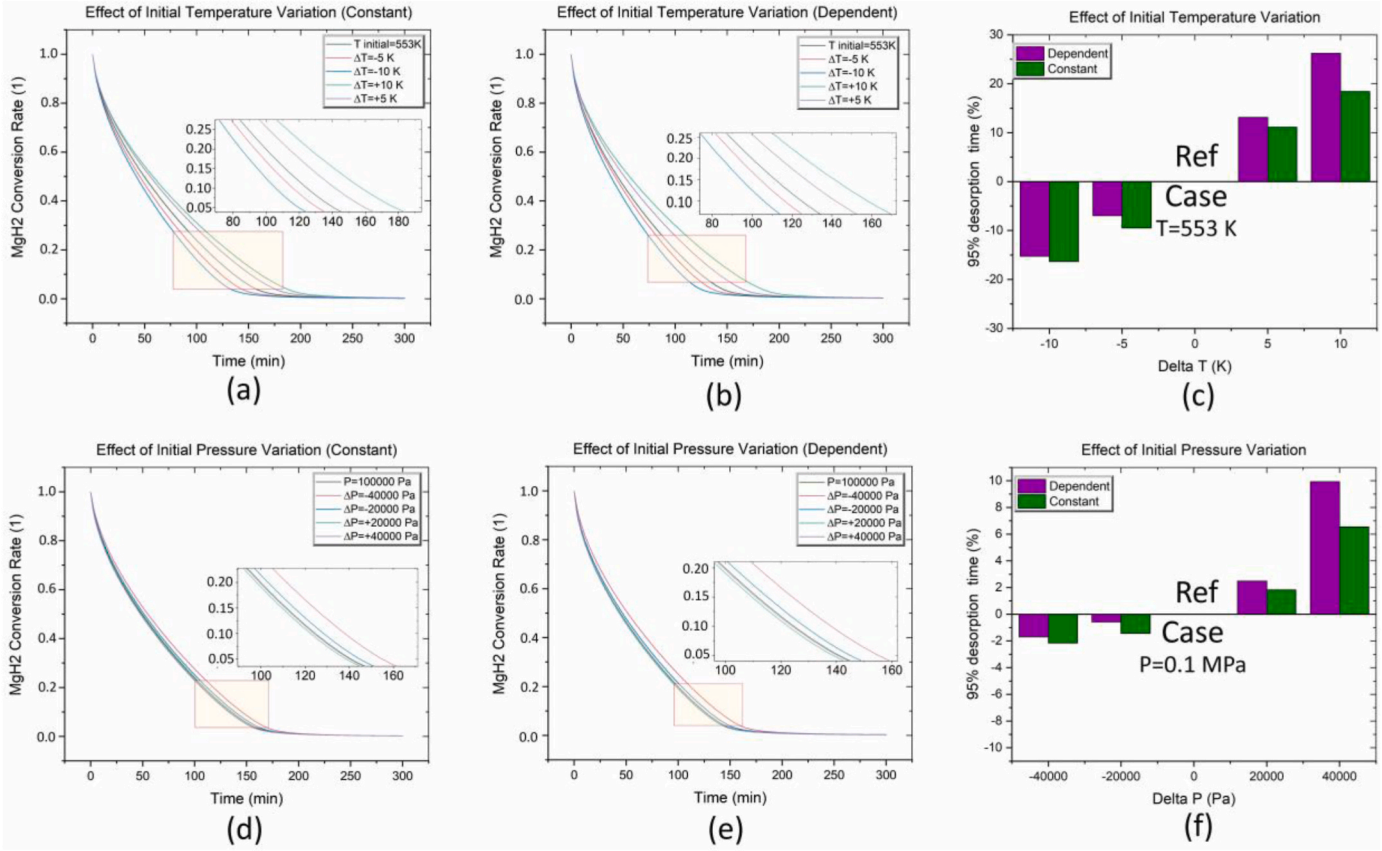

Fig. 13. Sensitivity analysis of initial conditions in the Thermochemical Storage System (TCSS).

thermal conductivity, compared to 15 % in the temperature-dependent case. An unexpected observation in the thermochemical storage system (TCSS) is that increasing the initial temperature leads to a longer hydrogen desorption time. This behavior can be attributed to the interaction between magnesium hydroxide $Mg(OH)_2$ and magnesium hydride MgH_2. Since $Mg(OH)_2$, has a lower thermal conductivity than MgH_2, it acts as a thermal barrier and limits the rate of heat transfer between the two materials. When the initial temperature increases, the thermal gradient between $Mg(OH)_2$, and MgH_2 becomes less pronounced, diminishing the driving force for heat flow and thus lowering heat flux. Additionally, while the hydration reaction ($MgO + H_2O \rightarrow Mg(OH)_2$) proceeds as expected, the heat it generates is finite due to the fixed quantities of water and MgO. At higher initial temperatures, a portion of this heat is used to elevate the surrounding temperature to the new baseline before any excess energy can be transferred to the MgH_2 layer. As a result, the effective thermal gradient driving heat flow toward the hydride becomes smaller, reducing heat transfer efficiency and slowing the desorption process. This behavior is consistent with the findings of Lutz et al. [32], who pointed out similar limitations due to the low thermal conductivity of $Mg(OH)_2$, a factor that delays the energy transfer to the MgH_2 region under adiabatic conditions.

On the other hand, the inherent low thermal conductivity of magnesium hydride results in the formation of steep thermal gradients during operation, particularly in systems without temperature-dependent conductivity adjustments. These steep gradients hinder uniform heat diffusion and act as a limiting factor in the overall desorption process. In temperature-dependent models, this issue is alleviated due to the adaptive nature of thermal conductivity, allowing the system to better respond to temperature variations and maintain more stable heat propagation. A similar trend is observed for pressure variations. When initial pressure is modified by ±20,000 Pa and ±40,000 Pa, desorption time increases with rising pressure. However, the magnitude of this effect is notably smaller compared to temperature variations, indicating that pressure fluctuations play a lesser role in controlling desorption kinetics. A 40,000 Pa increase extends desorption time by 9 % under temperature-dependent thermal conductivity and 6 % under constant thermal conductivity. These findings emphasize that temperature variations exert a stronger influence on desorption time than pressure changes, demonstrating the system's relative independence from pressure fluctuations. These findings highlight the necessity of incorporating temperature-dependent thermal conductivity in modeling thermochemical hydrogen storage, as it provides a more accurate and dynamic representation of system behavior. The results further highlight that temperature variations exert a stronger influence on desorption time compared to pressure changes, making thermal conductivity a key parameter in optimizing hydrogen storage performance.

3.4.2. *Parametric analysis for the radial heat flux system*

Fig. 14 examines how variations in initial temperature and pressure influence the hydrogen desorption process in a magnesium hydride storage system under radial heating conditions. The study evaluates how these factors affect desorption time and system performance under temperature-dependent and constant thermal conductivity models. To assess the impact of temperature variations, incremental changes of ±25 K and ±50 K were introduced.

A key observation is that the system exhibits greater sensitivity to temperature reductions than to increases, highlighting an asymmetrical response in desorption kinetics. For instance, lowering the initial temperature to 503 K (−50 K) extends the desorption time by 3 %, whereas increasing it to 603 K (+50 K) shortens the desorption time by just 1 %. This saturation effect suggests that beyond a critical temperature, further increases yield diminishing returns in desorption performance, as thermal conductivity variations become less influential at higher temperatures. It is also important to distinguish between the

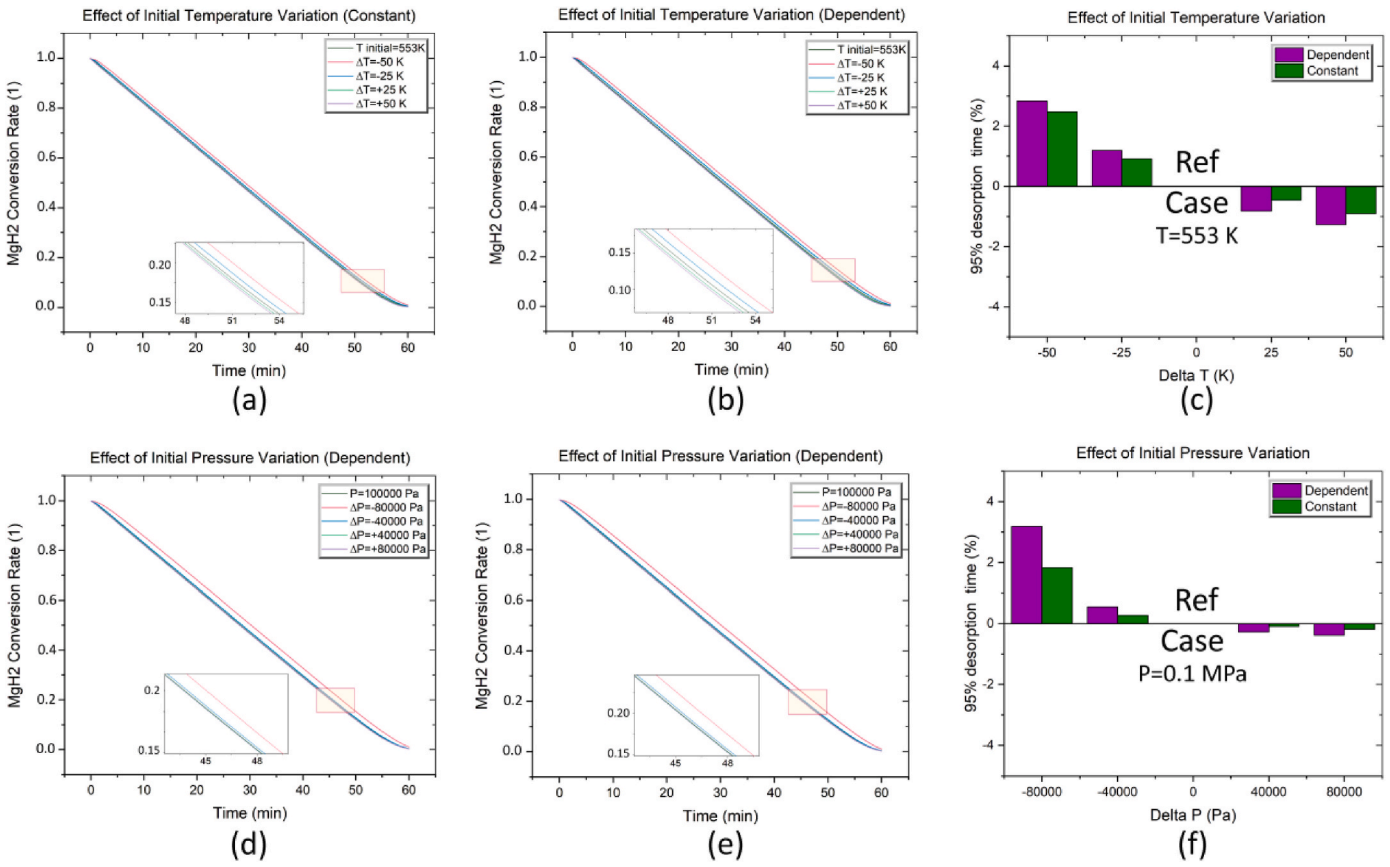

Fig. 14. Sensitivity analysis of initial conditions in the radial heat system.

temperature sensitivity of different system configurations. In the thermochemical storage system (TCSS), where hydrogen desorption depends entirely on the internally generated heat from hydration reactions, the process is highly sensitive to changes in initial temperature. Even a modest increase in temperature significantly weakens the thermal gradient and reduces the net available thermal energy for desorption. In contrast, the radial heat flux system receives a continuous external heat input, which maintains thermal propagation regardless of moderate initial temperature changes. As such, while a 10 K increase in TCSS significantly extends desorption time, a 50 K increase in the radial heat system leads to only a slight decrease in desorption duration. This highlights the dominant role of heat delivery mechanisms in governing temperature sensitivity. A similar trend is observed for initial pressure variations, which were adjusted by ±40,000 Pa and ±80,000 Pa. The system responds more strongly to pressure reductions than to increases. Lowering the initial pressure significantly extends desorption time due to the reduced pressure-driven force on hydrogen release. In contrast, increasing pressure beyond 80,000 Pa results in only a 0.7 % reduction in desorption time, despite the considerable energy input required. This highlights the inefficiency of excessive pressure increases for improving desorption performance. Overall, these results confirm that temperature changes have a much stronger effect than pressure variations on the radial heating system. While increasing both temperature and pressure can accelerate the desorption process, their effects diminish beyond a certain threshold, particularly for pressure. Optimizing initial temperature conditions is a more effective strategy than pressure adjustments for improving desorption efficiency, particularly under temperature-dependent thermal conductivity. These findings emphasize the need to prioritize thermal management strategies over pressure-based approaches when designing hydrogen storage systems for practical applications.

4. Conclusion

This study presents a comprehensive numerical investigation of the role of temperature-dependent thermal conductivity in hydrogen desorption from magnesium hydride. Through detailed modeling and validation, it demonstrates that assuming constant thermal conductivity significantly underestimates thermal gradient effects and introduces bias in predicting system behavior. In contrast, incorporating a temperature-dependent thermal conductivity model provides more accurate simulations of desorption time, thermal distribution, pressure evolution, and Darcy's velocity. In slow desorption processes, such as thermochemical storage systems, the temperature-dependent model reduced hydrogen diffusion time by approximately 9 min compared to the constant model. Under conditions of rapid radial heat flux, the reduction was about 0.6 min; however, even this seemingly small difference becomes critical in large-scale or continuous hydrogen storage systems. Furthermore, the temperature-dependent model improved equilibrium pressure predictions and enabled a more efficient thermal response, as confirmed by sensitivity analyses under various initial conditions. The key innovation of this work lies in developing thermal conductivity expressions based on experimental data. This addresses a gap in the literature, specifically the absence of a unified temperature-dependent formulation for magnesium hydride. This methodological advancement enables more accurate heat transfer modeling in metal hydrides and overcomes a long-standing limitation in hydrogen storage simulations. Compared to previous studies that have largely relied on constant thermal conductivity assumptions for computational simplicity, this study offers a more realistic and dynamic representation of heat transfer phenomena. By incorporating temperature-dependent formulations and assessing their impact across both slow and fast desorption scenarios, our model shows marked improvements in simulation accuracy and predictive capability. This modeling approach can

be extended in future work to other hydride materials and thermal enhancement techniques such as composite structures or multilayered designs. It may also be coupled with pressure-dependent models or integrated into real-time control algorithms to develop more intelligent and efficient hydrogen storage and delivery systems. Additionally, expanding experimental datasets across wider temperature and pressure ranges will further refine the model and broaden its applicability to real-world hydrogen energy systems.

Symbol	Expression	Unit
A	Arrhenius coefficient	$\frac{1}{s}$
T	Temperature	K
t	Time	s
λ	Thermal conductivity	$W/(m \cdot K)$
λ_{eff}	Effective thermal conductivity of the system	$W/(m \cdot K)$
ε	Porosity of the system (dimensionless)	–
$\lambda_{\text{gas}}(\mathbf{T})$	Thermal conductivity of hydrogen (temperature-dependent)	$W/(m \cdot K)$
$\lambda_{\text{MH}}(\mathbf{T})$	Thermal conductivity of metal hydride material (temperature-dependent)	$W/(m \cdot K)$
$\lambda_{\text{Hydrogen}}(\mathbf{T})$	Thermal conductivity of hydrogen as a function of temperature	$W/(m \cdot K)$
$\lambda_{\text{Steam}}(\mathbf{T})$	Thermal conductivity of steam as a function of temperature	$W/(m \cdot K)$
$\lambda_{eff(MgH_2)}$	Effective thermal conductivity of magnesium hydride	$W/(m \cdot K)$
$\lambda_{eff(Mg(OH_2))}$	Effective thermal conductivity of magnesium hydroxide	$W/(m \cdot K)$
ρ	Hydrogen density	kg/m^3
ρ_g	Gas phase density	kg/m^3
ρ_s	Solid phase density	kg/m^3
$(\rho C_P)_{eff}$	Effective heat capacity of the system	$J/(m^3 \cdot K)$
κ	Permeability	m^2
k	Reaction rate	$\frac{1}{s}$
$\partial T/\partial t$	Change of temperature with respect to time	K/s
u	Fluid velocity vector	m/s
∇T	Temperature gradient	K/m
$\nabla \cdot (k \nabla T)$	Heat flux due to conduction	W/m^3
$\dot{Q}$	Rate of heat production	W/m^3
C_P	Heat capacity at constant pressure	$J/(kg \cdot K)$
$C_{p,g}$	Specific heat capacity of the gas	$J/(kg \cdot K)$
$C_{p,s}$	Specific heat capacity of the solid	$J/(kg \cdot K)$
A	Arrhenius coefficient	$1/s$
E_a	Activation energy	J/mol
R	Gas constant	$J/(mol \cdot K)$
ΔH_r	Enthalpy change for the reaction process	J
ΔS_r	Entropy change for the reaction process	J/K
P_{eq,H_2}	Equilibrium pressure of hydrogen	Pa
P_{ref}	Reference pressure	Pa
v	Flow velocity	m/s
μ	Dynamic viscosity	$Pa \cdot s$
$\partial \rho/\partial t$	Change in hydrogen density over time	$kg/(m^3 \cdot s)$

CRediT authorship contribution statement

Davoud Abdi Lanbaran: Writing – review & editing, Writing – original draft, Visualization, Validation, Project administration, Methodology, Investigation, Formal analysis, Data curation, Conceptualization, davoud abdi lanbaran, Writing – review & editing, Writing – original draft, Visualization, Validation, Project administration, Methodology, Investigation, Formal analysis, Data curation, Conceptualization. **Chao Wang:** Supervision, Software. **Chuang Wen:** Writing – review & editing, Data curation. **Zhen Wu:** Writing – review & editing, Methodology. **Bo Li:** Writing – review & editing, Supervision, Software, Resources, Project administration, Funding acquisition.

Declaration of interest

The authors declare no conflicts of interest regarding this work. This research was conducted independently, without financial support, sponsorship, or affiliations that could have influenced the results.

References

[1] Neves AM, Puszkiel J, Capurso G, von Colbe JB, Klassen T, Jepsen J. Development of a new approach for the kinetic modeling of the lithium reactive hydride composite (Li-RHC) for hydrogen storage under desorption conditions. Chem Eng J 2023;464:142274.

[2] Ali M, Bibi Z, Younis MW, Majeed K, Afzal U, Khan S, Mubashir M. Enhancement of hydrogen storage characteristics of Na_2CaH_4 hydrides by introducing the Mg and Be dopant: a first-principles study. Int J Hydrogen Energy 2024;70:579–90.

[3] Ding N, Liu W, Chen B, Wang S, Zhao S, Wang Q, Cheng Y. Interface and body engineering via aluminum hydride enabling Ti-V-Cr-Mn alloy with enhanced hydrogen storage performance. Chem Eng J 2023;470:144143.

[4] Parida A, Prasad JS, Muthukumar P, Dalal A. A dynamic model for predicting the absorption and desorption behaviors of metal hydride systems and its implementation for screening of alloys for metal hydride hydrogen compressor. Int J Hydrogen Energy 2024;51:454–72.

[5] Potapov SN, Gvozdkov IA, Belyaev VA, Verbetsky VN, Mitrokhin SV. Magnesium hydride based hydrogen chemical source: development and application perspectives. Int J Hydrogen Energy 2019;44(54):28578–85.

[6] Li Q, Lu Y, Luo Q, Yang X, Yang Y, Tan J, Pan F. Thermodynamics and kinetics of hydriding and dehydriding reactions in Mg-based hydrogen storage materials. J Magnesium Alloys 2021;9(6):1922–41.

[7] Jain IP, Lal C, Jain A. Hydrogen storage in Mg: a most promising material. Int J Hydrogen Energy 2010;35(10):5133–44.

[8] Lang J, Eagles M, Conradi MS, Huot J. Hydrogenation rate limiting step, diffusion and thermal conductivity in cold rolled magnesium hydride. J Alloys Compd 2014;583:116–20.

[9] Ye J, Li Z, Zhang L, Wang S, Jiang L. Measurement and the improvement of effective thermal conductivity for a metal hydride bed–a review. RSC Adv 2022;12(39):25722–43.

[10] Dubey SK, Kumar KR. Charging and discharging analysis of thermal energy using magnesium nickel hydride based thermochemical energy storage system. Sustain Energy Technol Assessments 2022;52:101994.

[11] Busqué R, Torres R, Grau J, Roda V, Husar A. Mathematical modeling, numerical simulation and experimental comparison of the desorption process in a metal hydride hydrogen storage system. Int J Hydrogen Energy 2018;43(35):16929–40.

[12] Muhammed NS, Gbadamosi AO, Epelle EI, Abdulrasheed AA, Haq B, Patil S, Kamal MS. Hydrogen production, transportation, utilization, and storage: recent advances towards sustainable energy. J Energy Storage 2023;73:109207.

[13] Popilevsky L, Skripnyuk VM, Amouyal Y, Rabkin E. Tuning the thermal conductivity of hydrogenated porous magnesium hydride composites with the aid of carbonaceous additives. Int J Hydrogen Energy 2017;42(35):22395–405.

[14] Kumar EA, Madaria Y, Babu KS, Murthy SS. Influence of effective thermal conductivity on hydrogen sorption in Mg-$LaNi_{4.6}Al_{0.4}$ composite hydride beds for thermal energy storage. Therm Sci Eng Prog 2020;19:100653.

[15] Yoshida K, Noda S, Hanada N. Heat supply to and hydrogen desorption from magnesium hydride in a thermally insulated container with hot gas flow. Chem Eng J 2024;491:152070.

[16] Song M, Zhang L, Wu F, Zhang H, Zhao H, Chen L, Li H. Recent advances of magnesium hydride as an energy storage material. J Mater Sci Technol 2023;149:99–111.

[17] Thongtan P, Thiangviriya S, Utke O, Utke R. MgH_2-based hydrogen storage tank: kinetics, reversibility, and MWCNTs content. J Phys Chem Solid 2022;163:110578.

[18] Yoshida K, Kajiwara K, Sugime H, Noda S, Hanada N. Numerical simulation of heat supply and hydrogen desorption by hydrogen flow to porous MgH_2 sheet. Chem Eng J 2021;421:129648.

[19] Kumar N, Soren S. Magnesium metal nano composites—A solid state hydrogen storage material. Mater Today Proc 2023. https://doi.org/10.1016/j.matpr.2023.03.434.

[20] Malka IE, Bystrzycki J. The effect of storage time on the thermal behavior of nanocrystalline magnesium hydride with metal halide additives. Int J Hydrogen Energy 2014;39(7):3352–9.

[21] Albert R, Urbanczyk R, Felderhoff M. Thermal conductivity measurements of magnesium hydride powder beds under operating conditions for heat storage applications. Int J Hydrogen Energy 2019;44(55):29273–81.

[22] Larpruenrudee P, Bennett NS, Gu Y, Fitch R, Islam MS. Design optimization of a magnesium-based metal hydride hydrogen energy storage system. Sci Rep 2022;12(1):13436.

[23] Eisapour AH, Eisapour M, Talebizadehsardari P, Walker GS. An innovative multi-zone configuration to enhance the charging process of magnesium based metal hydride hydrogen storage tank. J Energy Storage 2021;36:102443.

[24] Bai XS, Rong L, Yang WW, Yang FS. Effective thermal conductivity of metal hydride particle bed: theoretical model and experimental validation. Energy 2023;271:127085.

[25] Shen D, Zhao CY. Thermal analysis of exothermic process in a magnesium hydride reactor with porous metals. Chem Eng Sci 2013;98:273–81.

[26] Afzal M, Mane R, Sharma P. Heat transfer techniques in metal hydride hydrogen storage: a review. Int J Hydrogen Energy 2017;42(52):30661–82.

[27] Reiser A, Bogdanović B, Schlichte K. The application of Mg-based metal-hydrides as heat energy storage systems. Int J Hydrogen Energy 2000;25(5):425–30.

[28] Parzinger S. 2014. Analytische Modellierung der temperatur- und gasdruckabhängigen effektiven Wärmeleitfähigkeit von Pulvern. Dissertation, Technische Universität München. Funded by the Bundesministerium für Wirtschaft und Technologie via DLR. Available at: https://www.epc.ed.tum.de.

[29] Bennett C, Eastwick C, Walker G. Effect of a varying effective thermal conductivity term on heat conduction through a physical model of a hydride bed. Int J Hydrogen Energy 2013;38(3):1692–701.
[30] Beattie SD, Harris A, Levchenko A, Rudolph J, Willson CD, McGrady GS. Thermal conductivity and specific heat measurements of metal hydrides. ITCC Proceedings 2009;11.
[31] Dong D, Humphries TD, Sheppard DA, Stansby B, Paskevicius M, Sofianos, Buckley CE. Thermal optimisation of metal hydride reactors for thermal energy storage applications. Sustain Energy Fuels 2017;1(8):1820–9.
[32] Lutz M, Bhouri M, Linder M, Bürger I. Adiabatic magnesium hydride system for hydrogen storage based on thermochemical heat storage: numerical analysis of the dehydrogenation. Appl Energy 2019;236:1034–48.
[33] Kim DM, Han DJ, Heo TW, Kang S, Wood BC, Lee J, Lee BJ. Enhancement of effective thermal conductivity of rGO/Mg nanocomposite packed beds. Int J Heat Mass Tran 2022;192:122891.
[34] Qureshi ZA, Ali HM, Khushnood S. Recent advances on thermal conductivity enhancement of phase change materials for energy storage system: a review. Int J Heat Mass Tran 2018;127:838–56.
[35] Kapischke J, Hapke J. Measurement of the effective thermal conductivity of a Mg–MgH_2 packed bed with oscillating heating. Exp Therm Fluid Sci 1998;17(4):347–55.
[36] Cooper JR, Dooley RB. The international association for the properties of water and steam. Proceedings of the international association for the properties of water and steam (IAPWS). 1993.
[37] Ishido Y, Kawamura M, Ono S. Thermal conductivity of magnesium-nickel hydride powder beds in a hydrogen atmosphere. Int J Hydrogen Energy 1982;7(2):173–82.
[38] Pohlmann C, Röntzsch L, Weißgärber T, Kieback B. Heat and gas transport properties in pelletized hydride–graphite-composites for hydrogen storage applications. Int J Hydrogen Energy 2013;38(3):1685–91.
[39] Marty P, de Rango P, Delhomme B, Garrier S. Various tools for optimizing large scale magnesium hydride storage. J Alloys Compd 2013;580:S324–8.
[40] Le-Quoc H, Coste M, Lacoste A, Laversenne L. Magnesium hydride films deposited on flexible substrates: structure, morphology and hydrogen sorption properties. J Alloys Compd 2023;955:170272.
[41] Madaria Y, Kumar EA, Murthy SS. Effective thermal conductivity of reactive packed beds of hydriding materials. Appl Therm Eng 2016;98:976–90.
[42] Bhouri M, Bürger I. Numerical investigation of H_2 absorption in an adiabatic high-temperature metal hydride reactor based on thermochemical heat storage: MgH_2 and $Mg(OH)_2$ as reference materials. Int J Hydrogen Energy 2017;42(26):16632–44.
[43] Shim JH, Park M, Lee YH, Kim S, Im YH, Suh JY, Cho YW. Effective thermal conductivity of MgH_2 compacts containing expanded natural graphite under a hydrogen atmosphere. Int J Hydrogen Energy 2014;39(1):349–55.
[44] Chaise A, De Rango P, Marty P, Fruchart D. Experimental and numerical study of a magnesium hydride tank. Int J Hydrogen Energy 2010;35(12):6311–22.
[45] Herbrig K, Röntzsch L, Pohlmann C, Weißgärber T, Kieback B. Hydrogen storage systems based on hydride–graphite composites: computer simulation and experimental validation. Int J Hydrogen Energy 2013;38(17):7026–36.
[46] Garrier S, Chaise A, de Rango P, Marty P, Delhomme B, Fruchart D, Miraglia S. MgH_2 intermediate scale tank tests under various experimental conditions. Int J Hydrogen Energy 2011;36(16):9719–26.
[47] Bogdanović B, Ritter A, Spliethoff B, Strabβurger K. A process steam generator based on the high temperature magnesium hydride/magnesium heat storage system. International Journal of Hydrogen Energy 1995;20(10):811–22.
[48] Li S, Yang X, Li X, Qu W, Zhou T, Dong T, Zhao J. A high energy density 3D nano-carbon based magnesium hydroxide reversible chemical reaction heat storage material synthesis and heat transfer performance investigation. J Energy Storage 2022;50:104260.
[49] Bhouri M, Bürger I, Linder M. Feasibility analysis of a novel solid-state H_2 storage reactor concept based on thermochemical heat storage: MgH_2 and $Mg(OH)_2$ as reference materials. Int J Hydrogen Energy 2016;41(45):20549–61.
[50] Zamengo M, Ryu J, Kato Y. Magnesium hydroxide–expanded graphite composite pellets for a packed bed reactor chemical heat pump. Appl Therm Eng 2013;61(2):853–8.
[51] Zamengo M, Ryu J, Kato Y. Thermochemical performance of magnesium hydroxide–expanded graphite pellets for chemical heat pump. Appl Therm Eng 2014;64(1–2):339–47.
[52] Zamengo M, Ryu J, Kato Y. Composite block of magnesium hydroxide–expanded graphite for chemical heat storage and heat pump. Appl Therm Eng 2014;69(1–2):29–38.
[53] Liang JZ. Thermal conductivity of PP/Al $(OH)_3$/Mg $(OH)_2$ composites. Compos B Eng 2013;44(1):248–52.
[54] Zamengo M, Ryu J, Kato Y. Chemical heat storage of thermal energy from a nuclear reactor by using a magnesium hydroxide/expanded graphite composite material. Energy Proc 2015;71:293–305.
[55] Zamengo M, Ryu J, Kato Y. Composite block of magnesium hydroxide–expanded graphite for chemical heat storage and heat pump. Appl Therm Eng 2014;69(1–2):29–38.
[56] Bennett CM, Patman AJ, Milanese C, Eastwick CN, Walker GS. Effect of powder characteristics for a magnesium based metal hydride store. Int J Hydrogen Energy 2014;39(34):19646–55.